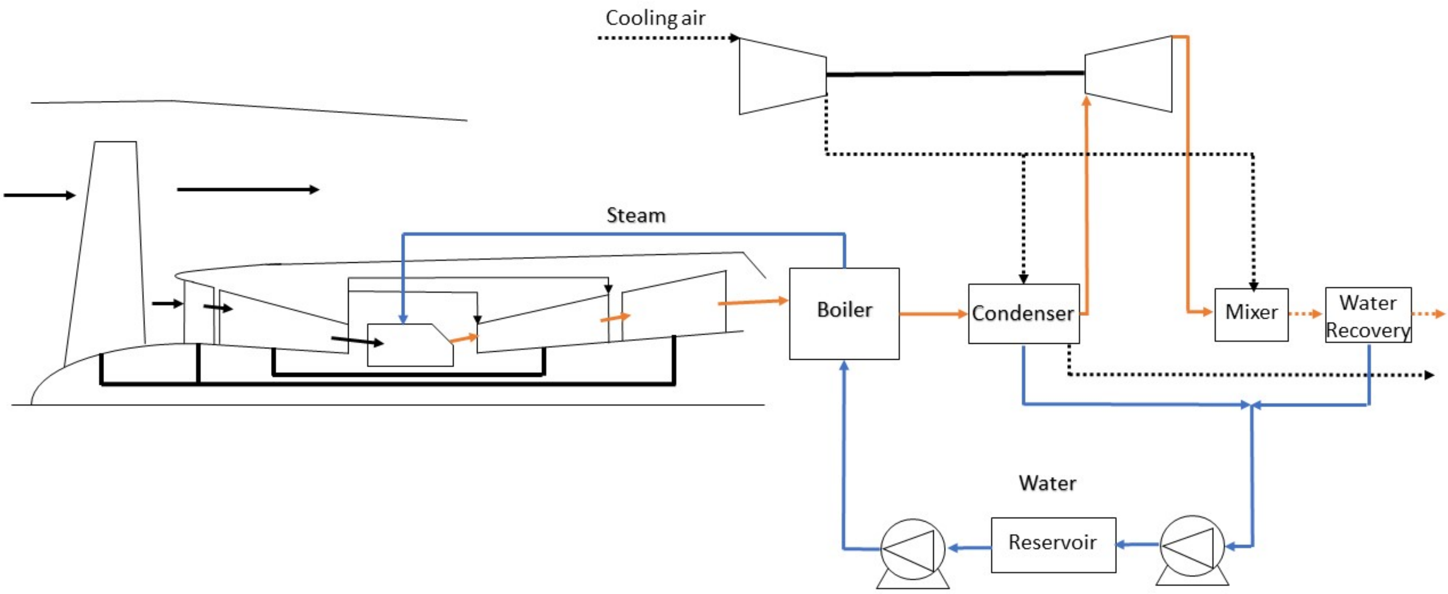

Steam generation and exhaust water recovery for the Water Enhanced Turbofan (WET)

Master's thesis in Sustainable Energy Systems

MERIM SAKIC

MICHAL NITULESCU

DEPARTMENT OF MECHANICS AND MARITIME SCIENCES
CHALMERS UNIVERSITY OF TECHNOLOGY
Gothenburg, Sweden 2021
www.chalmers.se

Master's thesis 2021

Steam generation and exhaust water recovery for the Water Enhanced Turbofan (WET)

MERIM SAKIC

MICHAL NITULESCU

Department Mechanics and Maritime Sciences
Division of Fluid Dynamics
Chalmers University of Technology
Gothenburg, Sweden 2021

Steam generation and exhaust water recovery for the Water Enhanced Turbofan (WET)

MERIM SAKIC
MICHAL NITULESCU

Supervisor: Anders Lundbladh, GKN Aerospace & Chalmers University of Technology
Examiner: Professor Tomas Grönstedt, Department of Mechanics and Maritime Sciences, Chalmers University of Technology

Master's Thesis 2021:60
Department of Mechanics and Maritime Sciences
Division of Fluid Dynamics
Chalmers University of Technology
SE-412 96 Gothenburg
Telephone +46 31 772 1000

Cover: Schematic representation of the investigated Water Enhanced Turbofan.

Typeset in LaTeX
Printed by Chalmers Reproservice
Gothenburg, Sweden 2021

Steam generation and exhaust water recovery for the Water Enhanced Turbofan (WET)

MERIM SAKIC
MICHAL NITULESCU
Department of Mechanics and Maritime Sciences
Chalmers University of Technology

Abstract

In order to combat the climate change, all industries must reduce their environmental impact. The aviation industry is no exception and new solutions must be found in order to make aircraft more environmentally friendly. One such solution could be the Water Enhanced Turbofan (WET), which is an engine concept presented by engineers at MTU Aero Engines in Germany [1] [2]. According to the authors, the engine concept promises a reduction of CO_2 emissions, NO_x emissions and formation of contrails [1].

This master's thesis investigates the potential of the WET concept during max cruise conditions from a thermodynamical perspective. The WET concept was applied to a conventional, simple cycle, turbofan, with GEnx-1B engine data generated by GESTPAN at Chalmers University of Technology. The WET concept utilizes steam injection and exhaust water recovery by the addition of two heat exchangers. The first heat exchanger, called the HRSG, heats the supplied water to steam which is injected into the combustion chamber. The second heat exchanger, called the condenser, is a plate heat exchanger where steam in the flue gas is condensed and separated. The HRSG could be designed with a weight of approximately 630 kg. The condenser was designed for several different configurations, but all different designs resulted in a weight of at least 3700 kg.

Results from this work show that the WET concept could reduce the SFC by up to 20 %, compared to a conventional turbofan, which is in somewhat alignment with the results published in the presenting articles [1] [2]. The addition of the heat exchangers resulted in a weight increase of the propulsion system by more than 70 % in relation to the original weight. A weight increase of 70 % of the propulsion system did not match the results in the article by MTU [1]. According to the authors of the MTU article, the total weight of the propulsion system was expected to increase by 40 %.

As a conclusion, it can be stated that theoretical results show that the WET concept has a potential to reduce emissions. However, for the WET concept to be implemented practically, thorough studies would have to be conducted on the condensation process in both the condenser and the mixer.

Acknowledgements

We would like to thank our supervisor, Anders Lundbladh, for all the help and advice throughout the master's thesis. Whenever we needed assistance, he always took the time for us. His vast knowledge, patience and will to discuss and explain has been invaluable to us.

We would also like to thank Oliver Sjögren, a PhD student at Chalmers, for his help with generating GEnx-1B data.

Finally we would like to express our gratitude to our examiner Tomas Grönstedt for his feedback and for granting us the opportunity to conduct this master's thesis.

Merim Sakic, Michal Nitulescu, Gothenburg, June 2021

Nomenclature

Abbreviations and terminology		
ΔP_C	Cold side pressure drop	
BPR	Bypass ratio	-
FAR	Fuel air ratio	-
FG	Flue gas	
FHV	Fuel heating value	J/kg
HPC	High pressure compressor	
HPT	High pressure turbine	
HRSG	Heat recovery steam generator	
LPC	Low pressure compressor	
LPT	Low pressure turbine	
PHX	Plate heat exchanger	
PR	Pressure ratio	-
RH	Relative humidity	-
Dimensionless numbers		
Nu	Nusselt number	-
Pr	Prandtl number	-
Re	Reynolds number	-
Variables and constants		
α	Temperature effectiveness	-
β	Heat capacity rate ratio	-
ΔH	Enthalpy change	J/kg
ΔT_{lm}	Logarithmic mean temperature difference	K
ΔT_m	Mean temperature difference	K
$\dot{m}$	Mass flow	kg/s
$\dot{x}$	Vapor quality	-
η_i	Isentropic efficiency	-
$\eta_{combustion}$	Combustion efficiency	-
λ	Heat capacity ratio	-
μ	Dynamic viscosity	Ns/m^2
$\rho^{''}$	Vapor density	kg/m^3
$\rho^{'}$	Liquid density	kg/m^3
ξ	Drag coefficient	-
A	Heat transfer area	m^2
C	Heat capacity rate	W/K
C_p	Isobaric heat capacity	J/(kg K)
d_i	Inner diameter	m

d_o	Outer diameter	m
D_e	Hydraulic diameter	m
F_{corr}	Correction factor	-
h_i	Inside heat transfer coefficient	$W/(m^2K)$
h_o	Outside heat transfer coefficient	$W/(m^2K)$
h_{GO}	Gas only heat transfer coefficient	$W/(m^2K)$
h_{id}	Inside dirt coefficient	$W/(m^2K)$
h_{LO}	Liquid only heat transfer coefficient	$W/(m^2K)$
h_{od}	Outside dirt coefficient	$W/(m^2K)$
j_f	Friction factor	-
k	Thermal conductivity	W/(m K)
L	Characteristic length	m
M_a	Flight mach number	-
P^*	Vapor pressure	-
P_c	Critical pressure	Pa
Q	Heat transferred per time unit	W
R	Gas constant	-
T_0	Stagnation temperature	K
T_a	Ambient temperature	K
T_c	Critical temperature	K
T_{FG}	Flue gas temperature	K
U	Overall heat transfer coefficient	$W/(m^2K)$
x_{vapor}	Vapor molar fraction	-
e	Absolute roughness	mm
M	Molar mass	g/mol
Q	Heat energy	W
R	Specific gas constant	J/(kg K)
v	Velocity	m/s
W	Work	W
w	Specie mass fraction	-

Contents

List of Figures

List of Tables

1

Introduction

1.1 Background

Aerospace engineering is recognized to be among the most advanced technology sectors in the world. The industry has seen significant improvement in aircraft performance and thus decreasing the environmental impact of each airplane [3]. The constant growth of the global aviation has nevertheless led to increasing amounts of emissions from the industry, and by 2018 it was responsible for 2.4% of the global CO_2 emissions [4]. The transport sector must reduce its emissions if we are to meet the climate targets and therefore new technologies must be implemented. Some ambitious goals have been set to reduce the impact by making advances in everything from engine efficiency to aircraft control centre logistics. One such goal is to reduce CO_2 emissions by 50% until 2050 compared to the year 2005 [5]. However airplanes do not only emit CO_2, they also contribute with for instance NO_x and water vapour. The emission of water vapour from airplane engines leads to formation of contrails and these contrails consist of small ice crystals, formed by the mixing of hot exhaust water vapour and the surrounding cold air. These contrails are easily distinguished by the characteristic white streaks that follow the airplane. Depending on atmospheric conditions, these ice crystals can quickly evaporate or they can remain and even grow [6] [7]. The total net forcing by the aviation industry was estimated to account for 5% of the total global warming in 2005. Non CO_2 terms, such as contrail cirrus, accounted for more than half of the aviation net effective radiation forcing [8].

To combat greenhouse emissions by the aviation industry, engineers at MTU Aero Engines in Germany proposed an engine concept called the Water Enhanced Turbofan (WET) [9], with the potential to lower emissions and fuel consumption [1]. According to MTU, the new technology has a potential to reduce CO_2 emissions by up to 15% and if sustainable fuel would be used, the reduction would be as high as 93% [2]. NO_x emissions could almost be entirely avoided and the contrail formation could potentially be reduced by as much as 90% [2]. The proposal from MTU was not a definite design of the WET engine, but a first analysis of the thermodynamical cycle with calculations on expected improvements compared to a modern and an expected evolutionary aeroplane by 2035. The analysis was performed on an Airbus A320 type aircraft [2].

The purpose of this work is to investigate, theoretically, the WET concept which has the potential of lowering aircraft greenhouse emissions. The proposed engine involves an already established concept of water injection within the combustion process. Water injection has traditionally been used to boost thrust at take-off and to lower NO_x emissions. The injected water is to be recovered to provide a fully self sufficient cycle, and to perform this two new heat exchangers are added. The first heat exchanger is a heat recovery steam generator and the second heat exchanger is a condenser.

1.2 Aim

The aim of the master's thesis is to investigate the potential of implementing the 'WET cycle' concept, with the GEnx-1B engine as base for calculations, from a thermodynamical perspective. Potential major problems with the implementation are to be identified and explained. The students will design two conceptual heat exchangers, one condenser and one HRSG, for max cruise conditions as it takes up most of the time for medium- and long-range flights. The condenser will be responsible for heat exchanging cold air with the flue gases, consequently condensing the present water vapour. The HRSG will be responsible for evaporating and superheating condensed water, by heat exchanging with the flue gases leaving the low-pressure turbine (LPT), which is then injected into the combustion chamber as steam.

1.3 Limitations

This work has had the aim to conceptually design two heat exchangers. The results do not include a complete conceptual design of the whole engine. As it is a first analysis of the concept, the requirements were not that we had to provide high resolution results for the complete cycle. To accomplish the design of the two heat exchangers, parameter optimization and further research would be needed to achieve a viable design. Furthermore, the work does not include dealing with the issue of practically integrating the heat exchangers within the structure of the aircraft except for basic suggestions of placement. It should also be noted that the work considers implementing the WET cycle on a GEnx-1B engine, meaning that the work does not guarantee that the suggestions, based on calculations, are valid for any other vehicle. The potential of optimizing the engine together with the WET concept is not investigated, but we believe it could result in extra benefits.

2
Theory

The modelling work is built upon several modules, such as the steam generator and condenser, where they are designed separately at first and then gradually connected towards the end. This theory section provides the basis for the calculations performed throughout this work in a step-by-step scheme. It will provide the necessary theoretical framework for all parts, from gas turbine cycles with cooling capabilities to the design of heat exchangers with the corresponding heat transfer coefficients and pressure drop. The gas turbine cycle is modelled and calibrated towards externally provided data from a gas turbine performance tool, GESTPAN.

2.1 General cycle

Before any studies on the WET cycle concept can be performed, a gas turbine model needs to be designed. The chosen cycle is a traditional Brayton cycle of turbofan type, and it has been tuned to match cycle data from a Chalmers model of the GEnx-1B engine (see 2.1.1 below). The engine architecture is a twin-spool engine where the fan and the booster (or low pressure compressor, LPC) are powered by the low pressure turbine (LPT), the high pressure compressor (HPC) is powered by the high pressure turbine (HPT). The combustion chamber is located in between the HPC and the HPT. In Figure 2.1, a schematic representation of the cycle is depicted.

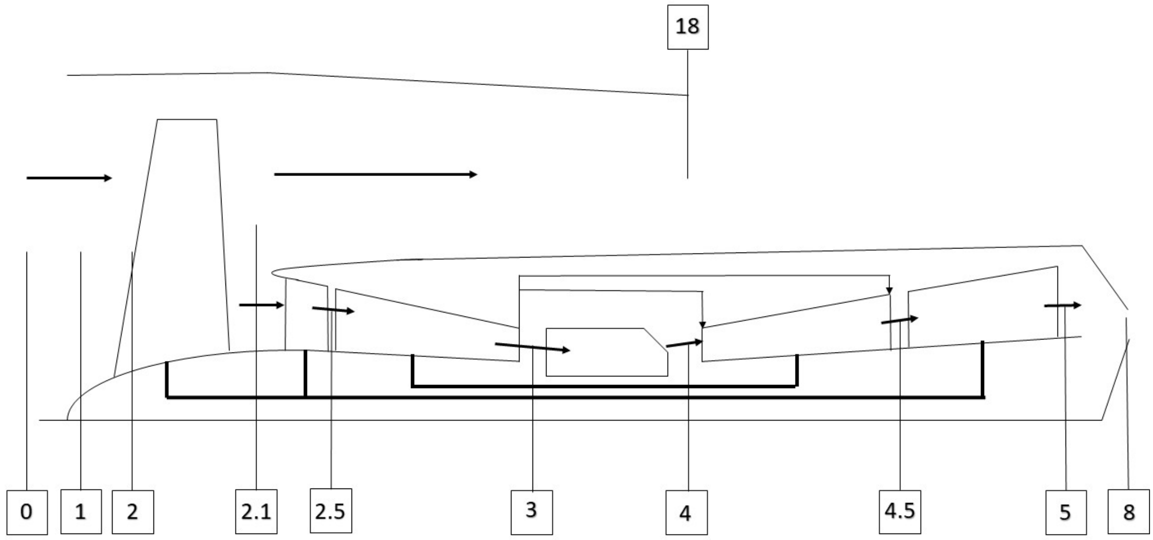

Figure 2.1: Schematic representation of a twin-spool turbofan engine (shafts represented with thick lines.

In Figure 2.1, some key areas of the cycle are marked with a number and these will be explained briefly before details for the calculations are provided.

The cycle seen in Figure 2.1 is a turbofan cycle using two spools (twin-spool) to power the compressing stages, with the shafts represented with thick lines. The fan and the low-pressure compressor has been attached to the shaft of the low-pressure turbine and the high-pressure compressor has been attached to the high-pressure turbine. Turbofan architecture usually involves several shafts as it is found to be more efficient to split the work between several turbine stages than connecting all the stages to a single shaft. When high pressure ratios are wanted and one shaft is used, severe breakdown of the flow in the compressor can occur if it is not operated within its design area [10]. The reason for this is that the gas at the inlet of a compressor will have a lower density than the gas at the exit of a compressor. To keep increasing the pressure, it would be aerodynamically convenient to provide a stage-by-stage increasing rotational speed. However, this is not mechanically possible and the compromise is to split the compression process into several spools.

Atmospheric air (station 0) is provided to the cycle via the fan at the entrance of the engine (station 2). Before the air goes through the fan, it passes the inlet (station 1) of the casing and the shear velocity of the aircraft will cause a pressure and temperature rise, which is referred to as ram pressure and ram temperature. The intake is a crucial part of an engine design as it has significant influence on aircraft safety and engine efficiency [10].

The air is split into two streams, one is directed towards the internal core of the engine, while the second portion will bypass the core of the engine and remain in a cooler state. The latter is referred to as the bypass stream which exits through the bypass nozzle (station 18). The core stream is compressed in several stages before it enters the combustion chamber (station 3), and is later expanded in the high-/low-pressure turbine (downstream of station 4). The expansion provides the necessary work and it powers the aircraft. After expansion it will be ejected via a core nozzle (station 8).

A modern aircraft engine uses blade cooling to keep the temperature of the blades at an adequate level. It has been noted that if the turbine inlet temperature is increased and the cooling air requirement is similar or constant, an increase of specific thrust and a decrease of specific fuel consumption (SFC) is possible [12]. It is however not only a matter of increasing the inlet temperature to achieve the benefits, the system would also need to be designed properly and optimized. The temperature increase can be achieved by supplying more fuel to the combustion chamber. The benefits of having higher inlet temperatures have led to the development of more efficient turbine blade cooling over the years. Without blade cooling the maximum allowed gas temperature is around 1000 ^{o}C, as the temperature then comes close to the melting point of the blade material. Using blade cooling, temperatures of 1800 ^{o}C can be achieved [12]. The blades are cooled by redirecting air from the high-pressure compressor to the interior of the high-pressure turbine blades, which are subjected to high temperatures. The cooling is performed both externally and internally [12]. This is represented by the two smaller arrows emanating from the end of the high-pressure compressor in Figure (2.1).

The thermodynamical investigation starts by modelling the incoming air to the engine inlet. To start one needs to know the aircraft altitude and get proper atmospheric conditions, which can easily be found in a lookup table such as the International Standard Atmosphere in literature.

The stagnation pressure and temperature at the inlet can be estimated with equation (2.1) and (2.2) [10],

$$\frac{T_{01}}{T_a} = [1 + \frac{\lambda - 1}{2} M_a^2] \tag{2.1}$$

$$\frac{P_{01}}{P_a} = [1 + \eta_{is}\frac{\lambda - 1}{2}M_a^2]^{\frac{\lambda}{\lambda-1}} \tag{2.2}$$

where η_{is} is the isentropic efficiency of the inlet. Equation (2.2) can be rewritten to equation (2.3) with the aid of equation (2.1) if one assumes that the inlet is isentropic.

$$\frac{P_{01}}{P_a} = \left(\frac{T_{01}}{T_a}\right)^{\frac{\lambda}{\lambda-1}} \tag{2.3}$$

The inlet will however always cause some losses, but it is usually very well designed as it has a significant part in making the cycle efficient and the aircraft safe [10]. The losses can be accounted for by assuming a small pressure ratio below unity for the component.

In the fan, the booster and the compressor section, the wanted pressure rise is specified in the form of a pressure ratio, PR, according to equation (2.4).

$$PR = \frac{P_{i+1}}{P_i} \tag{2.4}$$

With the pressure being determined via the pressure ratio, the exit temperature out of a compressing stage can be determined via the following iterative procedure.

$$T_{02.1}^{'} = T_{02}\left(\frac{P_{02.1}}{P_{02}}\right)^{\frac{\lambda-1}{\lambda}} = T_{02.1}\Big(PR\Big)^{\frac{\lambda-1}{\lambda}} \tag{2.5}$$

$$\Delta H^{'} = C_{p2.1}T_{02.1}^{'} - C_{p2}T_{02} \tag{2.6}$$

$$\Delta H = \Delta H^{'}\eta_{is} \tag{2.7}$$

$$T_{02.1} = \frac{\Delta H + C_{p2}T_{02}}{C_{p2.1}} \tag{2.8}$$

As can be noted from the procedure above, the isentropic efficiency is used in the computations instead of the polytropic efficiency. Normally the polytropic efficiency is preferred when using high pressure ratios, but in this work we model the engine around a fixed cycle (see section 2.1.1) and using the isentropic efficiency was preferred.

The procedure starts with equation (2.5) where the isentropic temperature (marked with a simple quotation mark) is computed. When the outlet temperature of equation (2.8) has been calculated, the procedure begins again with equation (2.6), where the isentropic temperature ($T_{02.1}^{'}$) is exchanged for the non-isentropic temperature ($T_{02.1}$). The iterative procedure continues until convergence has been reached. It is important to remember that the heat capacity is temperature dependent and should change for each iteration for a more accurate result. Note that the indices in equation (2.5) to (2.8) are set for the fan in Figure 2.1 (station 2 - 2.1), but the procedure is valid for both the booster/low-pressure compressor (station 2.1 - 2.5) and the high-pressure compressor (station 2.5 - 3).

To calculate the work required by the compressing stages, a mass flow through the engine is required. If the mass flow is unknown, one can temporarily employ a mass flow until the end stages when the thrust is to be computed. To calculate the work required by the compressing stages, the simple expression of equation (2.9) can be used,

$$W = \dot{m}_{core} \Delta H \tag{2.9}$$

where ΔH has been previously calculated with equation (2.7). The mass flow through the core, $\dot{m}_{core}$, can be found by setting a bypass ratio, BPR, in the engine. The bypass ratio is expressed according to equation (2.10) [10].

$$BPR = \frac{\dot{m}_{cold}}{\dot{m}_{core}} \tag{2.10}$$

With the compressing stages known, attention can be shifted towards the combustion chamber. To be able to calculate the amount of fuel required, a desired combustion temperature must be set. A simple energy balance can be placed around the combustion chamber according to equation (2.11).

$$\dot{m}_{air}(T_{in} - T_{ref})C_{p,air} + Q_{fuel}\eta_{combustion} = \dot{m}_{FG}(T_{out} - T_{ref})C_{p,FG} \tag{2.11}$$

The term $\eta_{combustion}$ is the combustion efficiency and takes into account that the combustion is not ideal and Q_{fuel} is the energy supplied by the combustion of fuel. Operational requirements often states that the combustion efficiency needs to be high and thus a high efficiency can be assumed [10]. The reference temperature is usually taken as 298 K [11]. Note that the heat capacities prior and after combustion are not the same as fuel has been added and thus the chemical composition has changed (for heat capacities, see 2.4.2). By recognizing that the term Q_{fuel} can be written according to equation (2.12),

$$Q_{fuel} = \dot{m}_{fuel} FHV \tag{2.12}$$

one can iterate over the fuel consumption and calculate the amount of necessary fuel. The term FHV is the fuel heating value, and it can be found in literature for different fuels.

There will be some pressure loss in the combustion chamber. Operational requirements often dictates that a pressure loss of 2-8 % is allowable in relation to the compressor working pressure [10]. Thus, a pressure ratio over the combustion chamber, below unity, can be assumed to account for this pressure loss.

The next part is to calculate the properties around the high- and low pressure turbine, which is downstream of station 4 to station 5 in Figure 2.1. With the required work defined by the compressing stages, one can compute the exit temperatures out of the expanding stages with equation (2.13) [10]. Note that the procedure is iterative if the heat capacity is not assumed constant.

$$W = m_{core} C_{p,mean} (T_{04} - T_{04.5}) \tag{2.13}$$

The required work defines the outlet temperatures, and the outlet temperature is used to calculate the outlet pressure from the turbines. Due to the non-isentropic nature of turbomachinery, a higher pressure drop will be observed than what is ideally expected and is accounted for with an isentropic efficiency. The pressure ratio over the turbines can be found according to equation (2.14) [10].

$$\frac{P_{04.5}}{P_{04}} = \left((T_{04} - \frac{T_{04} - T_{04.5}}{\eta_{is}}) \frac{1}{T_{04}} \right)^{\frac{\lambda}{\lambda - 1}} \tag{2.14}$$

Prior to solving the turbine section, blade cooling needs to be considered if it is to be applied. As mentioned previously, the cooling of the blades is an important aspect to the operation of the turbines. The approach, as can be seen in Figure 2.1, is to bleed some of the high-pressure compressor air from the end stage and direct it towards the high-pressure turbine. The method required to account for this accurately is very complex [10], thus a simplified approach will be used in this work. Prior to the flue gases entering the turbine (station 4), the flue gases are thought of as being mixed with a portion of the bleed cooling air and the temperature will consequently decrease. After expansion in the high pressure turbine there is a secondary addition of bleed air (station 4.5). The thermodynamical framework of the mixing process is that of an open type of system, and thus the expression is a simple energy balance over the mixture and is shown in equation (2.15),

$$T_{air} C_{p,air} m_{air} + T_{fg} C_{p,fg} m_{fg} = T_{mix} C_{p,air} m_{air} + T_{mix} C_{p,fg} m_{fg} \tag{2.15}$$

where T_{mix} is solved for in equation (2.15), which is the resulting temperature. Note that the solution is found through an iterative procedure. Alternatively, the right-hand side can be replaced by a single mixture term, but this requires calculation of the mixture properties such as heat capacity. The same equation is applied after the high-pressure turbine to compute the temperature after the second addition of cooling air.

When determining the thrust created by the cold and hot nozzles, it is necessary to know whether they are choked or not. If they are choked, this means that the Mach number at the exit cross section of the nozzle (station 8 and 18 in Figure 2.1) has reached unity. The following procedure considers the hot nozzle, but it is the same for the cold nozzle. Whether the nozzle is choked can be checked by comparing the pressure ratio between station 5 in Figure 2.1 and the ambient pressure ($\frac{P_{05}}{P_a}$) versus the pressure at station 5 with the critical pressure ($\frac{P_{05}}{P_c}$). The latter pressure ratio can be computed with equation (2.16) and is referred to as the critical pressure ratio [10],

$$\frac{P_{05}}{P_c} = \frac{1}{(1 - \frac{1}{\eta_{is}} \frac{\lambda - 1}{\lambda + 1})^{\frac{\lambda}{\lambda - 1}}} \tag{2.16}$$

where η_{is} is the isentropic efficiency of the nozzle. If $\frac{P_{05}}{P_a} > \frac{P_{05}}{P_c}$ the nozzle is considered choked and the Mach number has reached unity in the nozzle, otherwise it is not considered choked [10]. When choked, the static temperature and static pressure in the exit of the nozzle will be equal to the critical properties ($T_8 = T_c$ and $P_8 = P_c$) [10].

If the nozzle is choked, equation (2.17) can be used to solve for the critical temperature [10].

$$T_c = T_{05} - \eta_{is} T_{05} \left[1 - \left(\frac{1}{P_{05}/P_c} \right)^{\frac{\lambda-1}{\lambda}} \right] \tag{2.17}$$

If the nozzle is not choked, equation (2.18) can be used to solve for the nozzle temperature [10],

$$T_8 = T_{05} - \eta_{is} T_{05} \left[1 - \left(\frac{1}{P_{05}/P_8} \right)^{\frac{\lambda-1}{\lambda}} \right] \tag{2.18}$$

where $P_8 = P_a$ [10].

The velocity out of the nozzle can be determined via the definition of total temperature according to equation (2.19), where the velocity is solved for [10]. The static temperature was previously found with equations (2.17) if choked or (2.18) if not choked, and $T_{08} = T_{05}$.

$$T_{08} = T_8 + \frac{v_8^2}{2C_p} \tag{2.19}$$

With the velocity known, all hot side parameters are known, and with the procedure applied to the cold side, the thrust can be determined with equation (2.20) [10].

$$F_{net} = \dot{m}_{cold} C_{cold} + \dot{m}_{core} C_{core} - \dot{m} C_a + A_8 (P_8 - P_a) + A_{18} (P_{18} - P_a) \tag{2.20}$$

If the nozzles are chocked, then $P_8 = P_c$ and if the nozzle is not chocked, then $P_8 = P_a$. The same applies to the cold nozzle. It can be seen if the nozzles are unchoked, there is no pressure contribution to thrust.

The area of the nozzle can be determined via a continuity equation as in equation (2.21), where the area of the nozzle is solved for [10].

$$m = \rho V A_{nozzle} \tag{2.21}$$

The density can be found with the ideal gas law which is shown below in equation (2.22),

$$\rho = \frac{P}{RT} \tag{2.22}$$

where R is the specific gas constant. Note that the mass flows through the cold and hot nozzles are known as it was previously mentioned that a total mass flow could temporarily be set until the thrust is calculated. As the thrust can now be computed, the total mass flow can be varied until the designated thrust is achieved as specified by engine manufacturers.

The specific fuel consumption is a measurement of the efficiency and is defined as the ratio of the fuel consumption to the net thrust,

$$SFC = \frac{\dot{m}_{fuel}}{F_{net}} \tag{2.23}$$

where $\dot{m}_f$ is the fuel mass flow and F_{net} is the net thrust.

2.1.1 Calibration process of general cycle

The simple models presented above were put together in Excel and the model was tuned towards data provided from Oliver Sjögren, a PhD student from Chalmers [38]. The process of calibrating the cycle is vital as it enables more satisfactory results when the simple models used to describe the base cycle are used for the modified WET cycle. The calibration data originates from a Chalmers in-house simulation tool, GESTPAN, and aims to have agreement between properties such as the temperature and pressure at key points throughout the modelled cycle. The performance tool was developed by professor Tomas Grönstedt as a part of his doctoral thesis at Chalmers University of Technology [13].

2.1.2 Water Enhanced Turbofan (WET) cycle

With the theoretical framework of the general cycle established, the Water Enhanced Turbofan (WET) cycle is now to be implemented. As the name suggests the concept utilizes steam in the cycle where it is to be injected into the combustion chamber together with fuel and air. After the HPT and LPT the steam and flue gas mixture pass several heat exchangers where the water is recovered at the end stages of the WET cycle.

The use steam or water in a gas turbine cycle has been performed in the past. Such use today is mainly focused on ground based applications. Already in the beginning of the 20th century when the first gas turbines were developed, the injection of steam or water into the combustion chamber was a vital part for the proper function of the turbine. Water was used to reduce the peak temperatures in the equipment, which was required due to material limitations [14]. Water or steam injection in the combustion chamber for ground-based gas turbines is still an established method to reduce NO_x formation and was used for a long time [14]. The addition of water or steam reduces the oxygen content of the gas which causes the fuel to burn more slowly. In addition, the steam or water absorbs heat and reduces the peak combustion temperature which reduces the created amount of NO_x [14].

The injection of steam or water is not solely bound to the combustion chamber but can be introduced at different locations, such as the compressor inlet. When water is used in the compressor inlet, the power output increases as the water acts like a cooling media for the compressing fluid, thus reducing the compressor work [14]. Using water injection in aircraft engines has been studied and applied previously for thrust augmentation [15]. It has been extensively used in radial (reciprocating) engines where it served as an anti detonant so that more power could be drawn from the system without the danger of causing detonation in the engine [16]. It has also been used in aircraft gas turbines where it simply increased the thrust by adding more mass to the turbine flow. Also, the cooling effect is a positively contributing factor as it reduces the temperature of engine components. This principle has found applications at take-off where a significant thrust is needed but also for its cooling effect when the ambient temperature is high. These systems require on-board tanks to store water that is to be supplied to the engine, which in turn increases the weight of the airplane. It has not been used widely in modern engines [17].

The steam injecting and recovering cycle was, to the authors knowledge, first presented by MTU Aerospace in Germany for application within aerospace [1]. The architecture of the WET cycle is outlined in Figure 2.2.

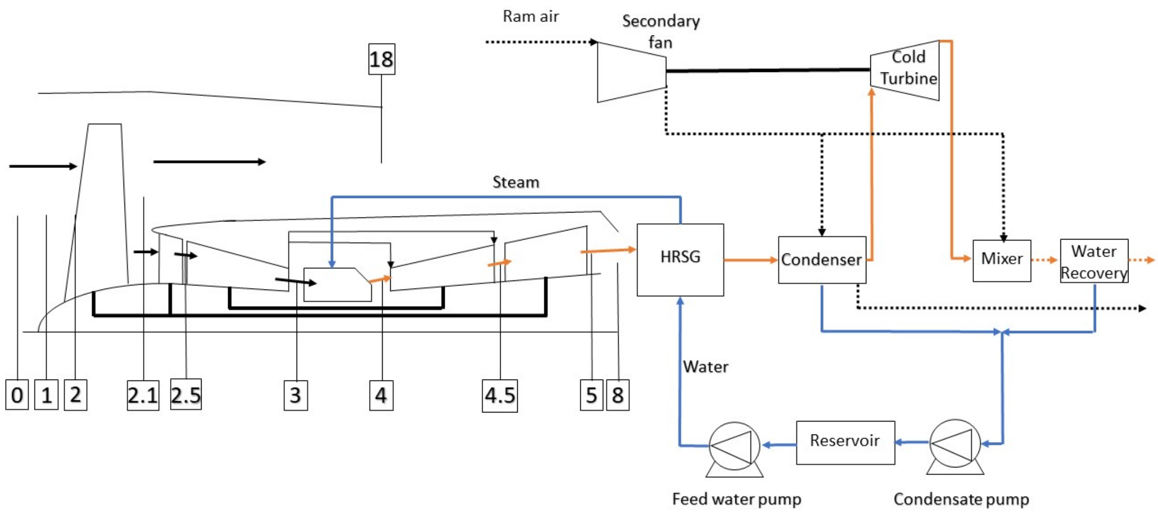

Figure 2.2: Schematic representation of the WET cycle in a twin-spool turbofan engine.

There are several benefits of utilizing the WET cycle in an aircraft, such as reduction of the SFC, reduction of NO_x-formation but also the reduction of fuel consumption [1]. The cycle contains a heat recovery steam generator (HRSG) for heating and evaporation of water and a two part condensation process which aims to recover the injected steam as condensate at the end stages of the cycle [1]. The cycle uses the hot exhaust gases of the engine to heat water and consequently evaporate and superheat it through the installation of the HRSG. This increases the overall efficiency as some of the waste heat is returned back to the cycle [14]. Water recovery is a crucial part of the cycle as it removes the need for the aircraft to carry additional water needed for injection. There is also the benefit of condensing the steam to water as the work required to increase the pressure to the combustion chamber pressure is much less for a liquid than a gas. Before the water is reused again it needs to be purified as it might contain solubles which might damage the gas turbine itself or the heat exchangers used [14].

Steam is injected into the combustion chamber where it is mixed with air and fuel. The flue gas and steam mixture pass through the turbines which power the compressing stages and then enters the HRSG section. The HRSG is placed immediately after the last turbine stage and it resides in the nacelle of the main engine [1]. In the HRSG, the flue gases exchange heat with the recovered water which consequently evaporates and is then superheated. According to the article [1] that proposed the WET concept, the water is supplied by an on-board feed water pump from an on-board reservoir. Alternatively, one could supply the water continuously as it is recovered. The cooled flue gases exit the HRSG and head towards the condenser through internal channels in the wing and then enter the condenser which is located inside the main fuselage of the aircraft, as proposed by the original concept article [1].

The condenser is plate heat exchanger, as proposed by the concept article [1], and ambient air is supplied as cooling media through a secondary fan. A large fraction of the injected water is recovered in the condenser, but not all. After the condenser, the flue gases enter a cold turbine and expand which in turn powers the secondary fan. It is important that the main engine cycle is constructed in such a way that there is sufficient pressure left so that the expansion in the cold turbine can power the secondary fan. This can be accomplished by increasing the combustion chamber temperature, thus adding more fuel, which results in a higher turbine inlet temperature and a smaller pressure drop in the turbine stages. It is also important to highlight that the injection of steam changes the chemical composition of the flue gases which has a thermodynamical effect on the cycle. Steam has a higher heat capacity than ordinary flue gases and thus a smaller pressure and temperature drop will be observed for the same work. The addition of steam influences γ and C_p which is covered in section 2.4.2.

After expansion, the flue gases are sent to a mixing area where additional steam will be extracted by mixing it with cold air. To uphold the cycle, all the injected water needs to be recovered. However, to decrease the amount of water vapor released into the atmosphere, additional water created in the combustion would also need to be extracted. The cold air absorbs the condensing heat from the condensation process of steam and is then ejected together with the flue gas through a nozzle. The heated cold air from the plate heat exchanger is ejected in a separate nozzle.

2.2 Heat Recovery Steam Generator

The heat recovery steam generator is a shell and tube heat exchanger, as proposed by the concept article [1]. In the following section the equations used for designing the HRSG are presented.

2.2.1 Heat transfer in tube bundle

A general equation for heat transfer across a surface is,

$$Q = UA\Delta T_m \tag{2.24}$$

where Q is heat transferred per unit time, U is the overall heat transfer coefficient, A is the heat transfer area and ΔT_m is the mean temperature difference.

The overall heat transfer coefficient, U, is calculated with all individual heat transfer coefficients that are relevant for the heat exchanging process:

$$\frac{1}{U} = \frac{1}{h_o} + \frac{1}{h_{od}} + \frac{d_o ln(\frac{d_o}{d_i})}{2k_w} + \frac{d_o}{d_i} \cdot \frac{1}{h_{id}} + \frac{d_o}{d_i} \cdot \frac{1}{h_i} \tag{2.25}$$

where h_o is the outside heat transfer coefficient, h_{od} is the outside dirt coefficient, k_w is the thermal conductivity of the tube wall material, h_i is the inside heat transfer coefficient and h_{id} is the inside dirt coefficient.

The LMTD method is one of the most common methods for designing heat exchangers and was chosen because of the known temperatures in the cycle. The log-mean temperature difference (LMTD) is defined as

$$\Delta T_{lm} = \frac{\Delta T_1 - \Delta T_2}{ln(\frac{\Delta T_1}{\Delta T_2})} \tag{2.26}$$

where index 1 and 2 is the inlet and outlet of the heat exchanger.

A requirement for using the LMTD method when designing the heat recovery steam generator is to divide it into three parts: an economizer, an evaporator, and a superheater. The reason for the split is that the temperature differences and overall heat transfer coefficient are different in the three parts of the HRSG.

The inlet flow area of the HRSG can be found with the mass continuity equation,

$$\dot{m} = \rho v A \tag{2.27}$$

by setting an allowable velocity. The total area of the HRSG inlet, which is the inlet flow area and the area of the tubes, is then dependent on the outer tube diameter and the tube pitch. The minimum thickness of the tubes, τ_t, to be able to withstand the internal pressure, is calculated with the following formula [20], referred to as Barlow's formula:

$$\tau_t = \frac{PD_o}{2(\sigma_\theta + P)} \tag{2.28}$$

where P is the internal pressure, D_o is the outside diameter of the tubes and σ_θ is the allowable hoop stress of the tube material.

With a known inlet flow area of the HRSG, known tube size and an expected heat exchanging area with an estimated overall heat transfer coefficient, it is possible to calculate the total size of the HRSG. With a known total size of the HRSG, the mass continuity equation is used to calculate the outlet velocity of the mixture composed of the flue gas and steam. The average velocity through the HRSG on the outside of the tubes is used to calculate the Reynolds number and the outer heat transfer coefficient.

The Reynolds number is defined as the ratio of inertial forces to viscous forces:

$$Re = \frac{\rho v L}{\mu} \tag{2.29}$$

where ρ is the fluid density, v is the fluid velocity, L is the characteristic length and μ is the dynamic viscosity.

The Prandtl number is defined as the ratio of momentum diffusivity to thermal diffusivity:

$$Pr = \frac{c_p \mu}{k} \tag{2.30}$$

where c_p is the isobaric specific heat capacity and k is the thermal conductivity.

The outer heat transfer coefficient is calculated through correlations and since the HRSG has an unusual flow pattern, correlations for flow across tube banks in a shell and tube heat exchanger are used. The used correlations are then compared and evaluated for calculation.

The Nusselt number is defined as the ratio of convective heat transfer to conductive heat transfer:

$$Nu = \frac{h}{\frac{k}{L}} \tag{2.31}$$

Zukauskas et al (1987) correlated data over large ranges of Re, Pr, transverse- and longitudinal pitch ratios, and presented the following expression for tube banks with staggered tube rows [21]:

$$Nu = 0.35 Re^{0.6} Pr^{0.36} (S_T/S_L)^{0.2} \tag{2.32}$$

where S_T is the transverse spacing between two tube centres and S_L is the longitudinal spacing between two tube centres.

VDI Heat Atlas states that the Nusselt number in a crossflow over a bundle of tubes can be calculated by multiplying a factor with the Nusselt number of flow around a single tube [22]. The Nusselt number of a single row is given by:

$$Nu_{l,0} = 0.3 + \sqrt{Nu_{l,lam}^2 + Nu_{l,turb}^2} \tag{2.33}$$

where the laminar Nusselt number is:

$$Nu_{l,lam} = 0.664 \sqrt{Re} Pr^{1/3} \tag{2.34}$$

and the turbulent Nusselt number is:

$$Nu_{l,turb} = \frac{0.037Re^{0.8}Pr}{1 + 2.443Re^{-0.1}(Pr^{2/3} - 1)} \tag{2.35}$$

The factor for a staggered tube arrangement is calculated by:

$$f_{stag} = 1 + \frac{2}{3b} \tag{2.36}$$

where b is the longitudinal pitch ratio. The Nusselt number in the tube bundle is calculated by:

$$Nu_{bundle} = f_{stag} Nu_{l,0} \tag{2.37}$$

2.2.2 Heat transfer in tubes

Inside the tubes the water is heated from subcooled liquid to overheated steam and the phase change has a large effect on the heat transfer. The water flowing through the tubes passes through several states. The water enters in a subcooled state and is then heated to its saturation point, which is referred to as the economizer section. When it has reached its saturation temperature it will start to boil, and this section is referred to as the evaporator. After it has evaporated, it will start to overheat, and this section is referred to as the superheater.

Ferguson and Eagle (1930) studied the heat transfer from tube to water [23]. Equation (2.38) is an adapted expression over the data from their work and can be used to determine the heat transfer coefficient within the economizer section. This equation has been developed specifically for water applications in tube flow,

$$h_i = \frac{4200(1.35 + 0.02T)u_t^{0.8}}{d_i^{0.2}} \tag{2.38}$$

where T is the water temperature (^oC), u_t (m/s) is the water velocity and d_i (mm) is the inside diameter of the tubes. As the water has been heated to a saturated state, boiling starts to occur. For the evaporator, VDI Heat Atlas presents correlations for both vertical and horizontal saturated boiling [24].

For flow boiling in a horizontal direction, equation (2.39) can be used,

$$\begin{aligned} \frac{h(z)_{conv}}{h_{LO}} = \Bigg[& (1-\dot{x})^{0.01}\Big((1-\dot{x}) + 1.2\dot{x}^{0.4}(\frac{\rho^{'}}{\rho^{''}})^{0.37}\Big)^{-2.2} \\ & + \dot{x}^{0.01}\Big(\frac{h_{GO}}{h_{LO}}(1 + 8(1-\dot{x})^{0.7}(\frac{\rho^{'}}{\rho^{''}})^{0.67})\Big)^{-2}\Bigg]^{-0.5} \end{aligned} \tag{2.39}$$

where $h(z)_{conv}$ is the convective heat transfer along the axis of movement, h_{LO} and h_{GO} are the logical heat transfer coefficients if the fluid remains as a liquid only (LO) or gas only (GO) and $\dot{x}$ is the vapor quality along the flow direction. $\rho^{'}$ is liquid density and $\rho^{''}$ is gas density.

For flow boiling in a vertical direction, equation (2.40) can be used.

$$\frac{h(z)_{conv}}{h_{LO}} = \Bigg[(1-\dot{x})^{0.01}\Big((1-\dot{x})^{1.5} + 1.9\dot{x}^{0.6}(\frac{\rho^{'}}{\rho''})^{0.35}\Big)^{-2.2} + \dot{x}^{0.01}\Big(\frac{h_{GO}}{h_{LO}}(1+8(1-\dot{x})^{0.7}(\frac{\rho^{'}}{\rho''})^{0.67})\Big)^{-2}\Bigg]^{-0.5} \tag{2.40}$$

Both vertical and horizontal boiling are of importance as the flow of water continuously change between these two conditions.

The procedure to acquire the heat transfer coefficient within the superheater section must also be considered. According to VDI Heat Atlas, the heat transfer for fully developed turbulent flow of gas (and liquid) within a pipe can be determined via equation (2.41) [22].

$$Nu_m = \frac{(\xi/8)RePr}{1+12.7\sqrt{\xi/8}(Pr^{2/3}-1)}[1+(d_i/l)^{2/3}] \tag{2.41}$$

This correlation is valid in the range of 10^4 < Re < 10^6, 0.1 < Pr < 1000. ξ can be determined via equation (2.42) and it is the drag coefficient [22].

$$\xi = (1.8log_{10}Re - 1.5)^{-2} \tag{2.42}$$

The heat transfer coefficient can then be determined via the definition of the Nusselts number, equation (2.31).

2.2.3 Pressure drop in tube bundle

The pressure drop must be taken into account and VDI Heat Atlas presents a procedure which can be used for preliminary estimation [25]:

$$\Delta P = \xi\eta_{MR}\frac{\rho v^2}{2} \tag{2.43}$$

where ξ is the drag coefficient and η_{MR} is the number of tube rows in the longitudinal direction. For a staggered tube arrangement the drag coefficient can be calculated with:

$$\xi = \xi_{lam} + \xi_{turb}F_v \tag{2.44}$$

where F_v is a factor which is dependent on the Reynolds number:

$$F_v = 1 - exp(-\frac{Re+200}{1000}) \tag{2.45}$$

The drag coefficient for the laminar flow is:

$$\xi_{lam} = \frac{f_{a,l,v}}{Re} \tag{2.46}$$

where $f_{a,l,v}$ is given by:

$$f_{a,l,v} = \frac{280\pi[(b^{0.5} - 0.6)^2 + 0.75]}{(4ab - \pi)a^{1.6}} \tag{2.47}$$

where a is the transverse pitch ratio and b is the longitudinal pitch ratio. The drag coefficient for the turbulent flow is:

$$\xi_{turb} = \frac{f_{a,t,v}}{Re^{0.25}} \tag{2.48}$$

where $f_{a,t,v}$ is given by:

$$f_{a,t,v} = 2.5 + \frac{1.2}{(a - 0.85)^{1.08}} + 0.4(\frac{b}{a} - 1)^3 - 0.01(\frac{a}{b} - 1)^3 \tag{2.49}$$

2.2.4 Pressure drop in tubes

The pressure drop inside the tubes is a complex process and a summation of several terms. There is friction due to movement of the fluid, there is evaporation and thus acceleration of fluid which causes pressure drop and there is further pressure drop due to bending. The pressure drop due to evaporation is considered to be small, while the static pressure drop is not considered as the correlations found in VDI Heat Atlas [25] were out of the scope of this study. This work will thus only account for the frictional pressure drop.

The isothermal pressure drop due to friction can be expressed according to equation (2.50) [23].

$$\Delta P = 8\xi \left(\frac{L}{d_i}\right) \rho \frac{u_t^2}{2} \tag{2.50}$$

However, the temperature will not remain constant in the heat exchanger except when the fluid is evaporating. To account for the economizer and superheater section, equation (2.51) can be used which accounts for the change in physical properties via the difference of viscosity between the bulk flow and the flow closest to the wall [23],

$$\Delta P = 8\xi \left(\frac{L}{d_i}\right) \rho \frac{u_t^2}{2} \left(\frac{\mu}{\mu_w}\right)^{-0.14} \tag{2.51}$$

where L is the length of the computed section. The drag coefficient, ξ, can be found with an iterative approach according to equation (2.52) [27],

$$\frac{1}{\sqrt{\xi}} = -2.5ln(0.27\frac{e}{d_i} + 0.885Re^{-1}\xi^{-0.5}) \tag{2.52}$$

where e (mm) is the absolute roughness of the used material. To account for the frictional pressure drop in the evaporator section, one can compute the pressure drop as if liquid and gas only and use a mean of these values. Note that the phase change from water to steam leads to a higher velocity and this might induce a higher pressure drop.

2.3 Condenser and water recovery system

The water contained in the flue gases is to be recovered through a water recovery system. This is performed in a twostep condensation process of which the first step consists of a plate heat exchanger (PHX), as stated in the article [1], and the second step consists of an open heat exchanging process, referred to as the mixer. An additional component is the cold turbine which will expand the remaining pressure in the flue gases and produce work to power a secondary fan which provides necessary cooling air. The placement of these components can be seen in the article [1].

The first step, the PHX, is responsible for extracting a large amount of the water contained within the flue gases. The heat exchanger architecture will play a vital role when dimensioning the heat exchanger. The second step, the mixer, is responsible for extracting the rest of the desired water which is performed by mixing cold air with the flue gases exiting the cold turbine.

The process of condensation, both in the condenser and the mixer, is dependent on the vapor pressure of steam in the flue gases. To extract a certain amount of water, a specific vapor pressure needs to be achieved, and thus the temperature out of the condenser is automatically set. For calculations on the vapor pressure and its temperature dependency, see section 2.4.3.

The vapor pressure exerted by the steam in the flue gases (as an ideal case) at any time can be expressed with equation (2.53) [26],

$$P_{vapor} = P_{total} x_{vapor} \tag{2.53}$$

where x_{vapor} is the molar fraction of steam in the flue gases and can be calculated according to equation (2.54),

$$x_{vapor} = \frac{\frac{m_{steam}}{M_{water}}}{\frac{m_{FG}}{M_{FG}} + \frac{m_{steam}}{M_{water}}} \tag{2.54}$$

where uppercase M is the molar mass of the flue gases and water.

To condense a specific fraction of the water, a new molar fraction and vapor pressure will be achieved, see equation (2.55), and thus the target vapor pressure can be calculated according to equation (2.53),

$$x_{vapor,target} = \frac{\frac{m_{steam} - m_{steam} X_{condensed}}{M_{water}}}{\frac{m_{FG}}{M_{FG}} + \frac{m_{steam} - m_{steam} X_{condensed}}{M_{water}}} \tag{2.55}$$

where the hot stream temperature out of the heat exchanger is expressed according to equation (2.56) and can be found by using equations from section 2.4.3, which correlates vapor pressure to temperature.

$$T_{condenser}^{out,hot} = T(P_{vapor,target}) \tag{2.56}$$

Figure 2.3 contains a graphical representation of the water recovery system and its function through a vapor pressure diagram.

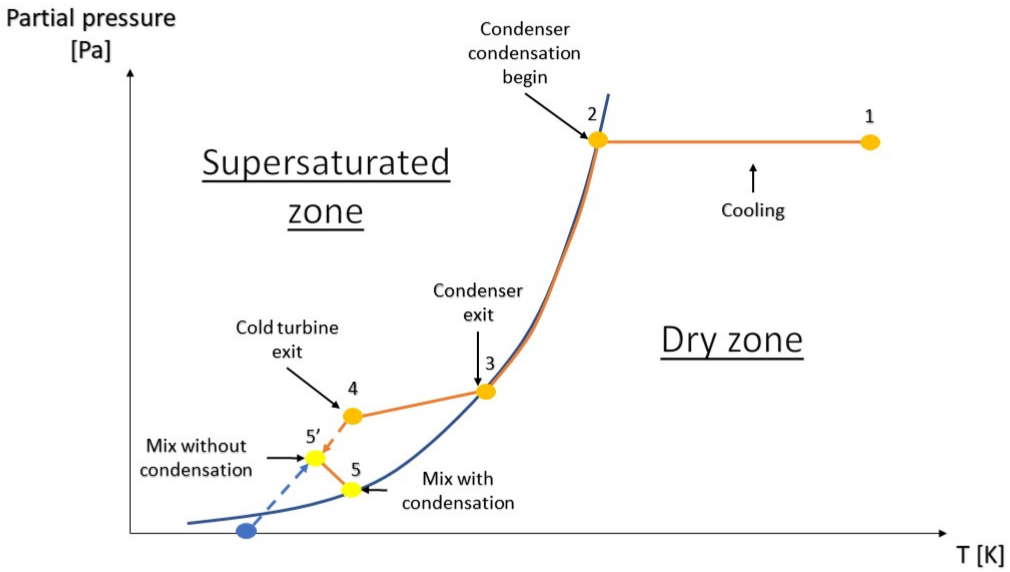

Figure 2.3: The conceptual pathway of the exhaust flow within the water recovery system, depicted in a vapor pressure diagram.

In Figure 2.3, the blue line represents the water vapor pressure, which is as a function of the temperature, and the orange line represents the pathway of the cooling process. After the heat recovery steam generator, the flue gases enter the condenser (point 1) and are first cooled down to the saturation temperature (point 2). When the temperature has reached the vapor saturation temperature, steam will start to condense out of the flue gases until a certain exit temperature is reached, which is defined by the designer (point 3).

After exiting the condenser, the flue gases enter the cold turbine where they expand, and the pressure and temperature will be reduced (point 4). This will put the flue gases in a supersaturated state after the cold turbine and the steam will start to condense again.

Condensation releases heat to the surroundings which is to be absorbed by the cooling air. After the flue gases have left the cold turbine, they will mix with cooling air (blue dot). If no condensation would occur, point 5' would be reached. But due to the supersaturation of the exhaust flow, and the addition of cold air, steam will continue to condense and theoretically point 5 will be reached. Depending on the amount of cooling air supplied, the temperature of the mixture might increase or decrease in relation to the cold turbine exhaust. In reality, the residence time of the flue gases in the mixing section might not be sufficient to reach equilibrium, which is when the relative humidity is equal to 1, and the exiting flow will be supersaturated. As the cold air and the flue gases are mixed, the partial pressure of steam in the mixture will decrease.

When designing the heat exchanger, the heat process can be depicted in a duty-temperature diagram as in Figure 2.4.

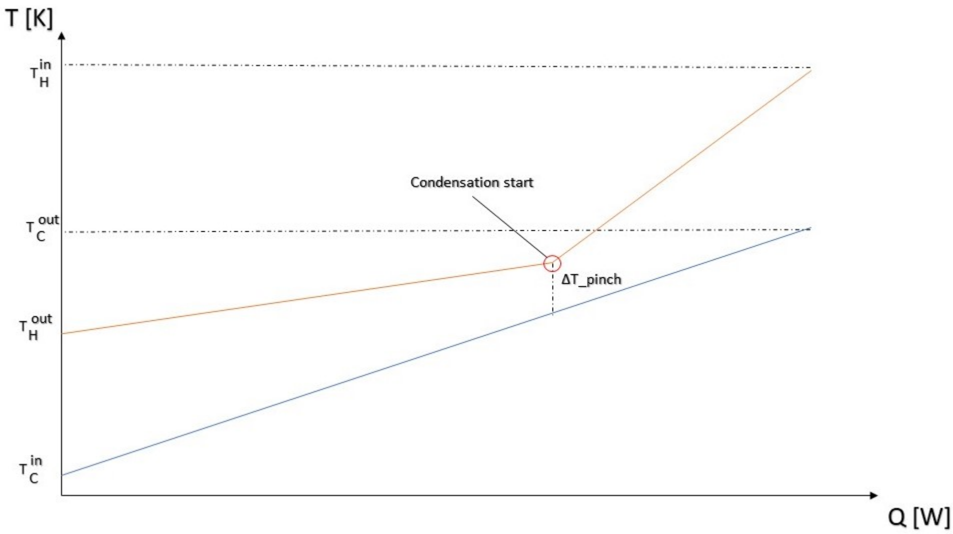

Figure 2.4: Depiction of the heat process conducted in the condenser of a binary mixture (red line) and cooling media (blue line).

In Figure 2.4, it can be seen that the cooling process temperature drop is substantially higher than the condensing temperature drop. When designing the condenser, the duty should be segmented into two parts for the LMTD procedure to be viable. The outlet temperature of the cooling air is harder to predict and is highly affected by the heat exchanger architecture. This parameter needs to be properly defined and a pinch temperature needs to be determined. The pinch temperature is the minimum allowable temperature difference at any point between the two heat exchanging fluids. A consequence of using plate heat exchangers is that low pinch temperatures can be reached, as low as 1^oC are possible [23].

2.3.1 Plate heat transfer and pressure drop

Plate heat exchangers are easy to handle, compact and come in various shape and sizes. The estimation of the thermal performance can seem to be hard to determine due to the complexity and variation of configurations. Of the available configurations, the Chevron type plate heat exchanger is the most common type where parameters such as amplitude, wavelength and the Chevron angle can be varied [28].

For the most common type of plate heat exchangers, equation (2.57) can be used to estimate the thermal performance [29].

$$Nu = 0.374Re^{0.668}Pr^{0.33}\left(\frac{\mu}{\mu_w}\right)^{0.14} \tag{2.57}$$

The heat transfer coefficient can then be found be using equation (2.31). By calculating the heat transfer coefficient on both the hot and cold stream of the condenser, the overall heat transfer, U, can be found with equation (2.25).
The pressure drop is strongly affected by the shape and geometry of the plates, in this work the frictional pressure drop is considered and equation (2.58) can be used to calculate it [30],

$$\Delta P = 8j_f\left(\frac{L_p}{D_e}\right)\frac{\rho v^2}{2} \tag{2.58}$$

where the friction factor j_f is estimated by using equation (2.59) [30],

$$j_f = 0.6Re^{-0.3} \tag{2.59}$$

The Reynolds number for a plate heat exchanger is calculated by using equation (2.60) [30],

$$Re_p = \frac{\rho v D_e}{\mu} \tag{2.60}$$

where D_e is the equivalent (hydraulic) diameter and can be taken as twice the gap between the plates. The velocity over the plates is found by equation 2.61.

$$\dot{m}_{cold} = \rho v A_{gap} \tag{2.61}$$

where A_{gap} is determined by setting the dimensions between the plates (width and height). To find the required cold mass flow, equation (2.62) is used.

$$\dot{m}_{cold} = \frac{Q}{C_{p,air}\Delta T_c} \tag{2.62}$$

To estimate the duty required over the condenser, equation (2.24) is used. It is important to define the temperature difference in an appropriate way. The temperature difference, which is the driving force, varies depending on the flow arrangement of the heat exchanger. The driving force is expressed by equation (2.63),

$$\Delta T_m = F_{corr}\Delta T_{lm} \tag{2.63}$$

where the correction factor, F_{corr}, is a measurement of the deviation from an ideal case, a counter current case [31]. The estimation procedure of the correction factor is presented in section 2.3.1.1. The duty in the condenser is then expressed in the following way.

$$Q = UA_{total}F_{corr}\Delta T_{lm} \tag{2.64}$$

By solving for the total area in the PHX, A_{total}, the number of required plates is found by equation (2.65),

$$N_{plates} = \frac{A_{Total}}{A_{Plate}} \tag{2.65}$$

where the plate area, A_{plate}, is the area of each plate. The mass flow through each plate intake can then be found accordingly.

$$\dot{m}_{plate} = \frac{2\dot{m}_{total}}{N_{plates}} \tag{2.66}$$

And is applied to both the cold and hot side mass flows.

2.3.1.1 Correction factor

The correction factor in LMTD heat exchanger analysis relates how the investigated heat exchanger deviates from an ideal case. The correction factor can take values between 0 and 1, where 1 is the ideal case of a counter current heat exchanger [31]. The following procedure was originally created for shell and tube heat exchangers, but it can be adapted for crossflow heat exchangers. More accurate methods could be concieved, but due to the lack of available estimation procedures for plate heat exchangers, it can be used to estimate an approximate correction factor.

To estimate the correction factor, the cold and hot side heat capacity rates are to be computed as in equation (2.67) and (2.68) [32].

$$C_1 = \dot{m}_1 C_{p,1} \tag{2.67}$$

$$C_2 = \dot{m}_2 C_{p,2} \tag{2.68}$$

The next parameter that needs to be estimated is the temperature effectiveness, α, for both the cold and hot side [32],

$$\alpha_1 = \frac{T_{1,o} - T_{1,i}}{T_{2,i} - T_{1,i}} \tag{2.69}$$

$$\alpha_2 = \frac{T_{2,i} - T_{2,o}}{T_{2,i} - T_{1,i}} \tag{2.70}$$

where the index **1** and **2** reefer to fluid 1 and fluid 2 (hot and cold) and the index ***i*** and ***o*** reefer to inlet and outlet. The heat capacity rate ratio, β, is also needed for the estimation of the correction factor and can be computed by equation (2.71) and (2.72) [32].

$$\beta_1 = \frac{T_{2,i} - T_{2,o}}{T_{1,o} - T_{1,i}} \tag{2.71}$$

$$\beta_2 = \frac{T_{1,o} - T_{1,i}}{T_{2,i} - T_{2,o}} \tag{2.72}$$

The correction factor can be estimated with the following equations. Equation (2.73) is used when fluid 1 is in a mixed state and fluid 2 in an unmixed state in a single pass crossflow exchanger. Equation (2.74) is used when fluid 2 is in a mixed state and fluid 1 in an unmixed state in a single pass cross flow exchanger [32].

$$F_{corr} = \frac{ln\Big[(1-\beta_1\alpha_1)/(1-\alpha_1)\Big]}{(\beta_1 - 1)ln\Big[1 + (1/\beta_1)ln(1-\beta_1\alpha_1)\Big]} \tag{2.73}$$

$$F_{corr} = \frac{ln\Big[(1-\beta_1\alpha_1)/(1-\alpha_1)\Big]}{(1 - 1/\beta_1)ln\Big[1 + \beta_1 ln(1-\alpha_1)\Big]} \tag{2.74}$$

2.3.1.2 Condenser size

The condenser operating temperature is significantly lower than in the HRSG and for this reason a lighter material such as aluminium can be used to achieve a lower condenser weight. A low plate thickness is also desired as it will further reduce the required weight of the condenser.

2.3.2 Cold Turbine

After the condenser, the cold air is redirected towards a cold turbine where the turbine is designed to power the secondary fan. A positive outcome of the turbine is that the decrease in pressure will also decrease the temperature. The temperature out of the turbine can be calculated using equation (2.75) [10].

$$T_{02} = (T_{01}\Big(\frac{1}{PR}\Big)^{\frac{\lambda-1}{\lambda}} - T_{01})\eta_{is} + T_{01} \tag{2.75}$$

2.3.3 Secondary fan

The secondary fan is placed on the same axis as the cold turbine and its prime purpose is to supply air for the condensation process. It also works as a work sink for the work produced by the cold turbine. The temperature rise by the secondary fan can be calculated according to equation (2.3).

2.3.4 Mixer

After the cold turbine, the flue gases mix with cold air which will initiate further condensation. The air for mixing is supplied by the secondary and the mixer is an open type heat exchanger.

By predetermining the fraction of water that is to be condensed in the mixer section, the required air mass flow is found. To perform these calculations, equation (2.76) is used. The calculations for the mixer section are complicated as there are several ongoing processes at the same time. Also, the inlet and outlet temperatures need to be properly defined, or calculated depending on what approach the designer applies. The velocity of the cooling air is free to be set by the designer, but care needs to be taken as any deceleration of the cold air will increase the temperature. The required cooling air can be estimated with equation 2.76.

$$C_{p,air}\dot{m}_{air}T_{air,in} + C_{p,exhaust}\dot{m}_{exhaust}T_{exhaust,in} = C_{p,mix}\dot{m}_{mix}T_{mix,out} + Q_{condensation} + Q_{steam,cool} \tag{2.76}$$

The outlet temperature of the mixture corresponds to a specific vapor pressure and to extract water through condensation, the outlet temperature must be low enough for the relative humidity to be equal to or larger than 1.

When the cold air is mixed with the warmer flue gases, not only will there be a heat exchange due to condensation, but also due to the temperature differences between the flows. Figure 2.5, shows a illustrative representation of the nozzle where mixing occurs. Note that the condensation is not represented in Figure 2.5 but only the gaseous flow which will mix.

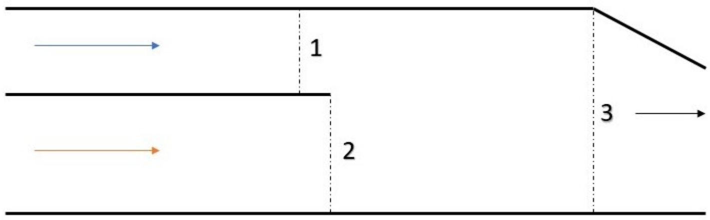

Figure 2.5: Depiction of the mixing in the nozzle. The cold air, represented by the blue arrow, enters from the secondary fan and the flue gases, represented by the orange arrow, exit the cold turbine and head towards the mixer.

A procedure will now be presented on how to calculate the mixing properties when two streams are mixed. The following procedure will assume adiabatic flow with no losses [10].

A total enthalpy balance on the system in Figure 2.5 yields equation (2.77) [10].

$$\dot{m}_1 C_{p,1} T_{01} + \dot{m}_2 C_{p,2} T_{02} = \dot{m}_3 C_{p,3} T_{03} \tag{2.77}$$

The properties at station 3, in Figure 2.5, is dependent on its constituents station 1 and station 2 [10],

$$C_{p,3} = \frac{\dot{m}_1 C_{p,1} + \dot{m}_2 C_{p,2}}{\dot{m}_1 + \dot{m}_2} \tag{2.78}$$

$$R_3 = \frac{\dot{m}_1 R_1 + \dot{m}_2 R_2}{\dot{m}_1 + \dot{m}_2} \tag{2.79}$$

$$\lambda_3 = \frac{C_{p,3}}{C_{p,3} - R_3} \tag{2.80}$$

where R is the specific gas constant.

A momentum balance of the system in Figure 2.5 is expressed as:

$$(\dot{m}_1 v_1 + P_1 A_1) + (\dot{m}_2 v_2 + P_2 A_2) = \dot{m}_3 v_3 + P_3 A_3 \tag{2.81}$$

The static pressures of the two mixing flows can be set equal if one assumes that there is no direct swirl in the jet pipe downstream [10]. The static pressure and temperature for the cold stream will depend on the velocity of the stream, which is a parameter determined by the designer.

The Mach number of the hot flue gas stream exiting the cold turbine is expressed by rewriting equation (2.2).

$$M_2 = \sqrt{\left(\left(\frac{P_{02}}{P_2}\right)^{(\lambda-1)/\lambda} - 1\right)\frac{2}{(\lambda-1)\eta_{is}}} \tag{2.82}$$

With the velocities and mass flows known, the duct area at station 1 and station 2 is found with a mass continuity balance, with the density derived from the ideal gas law. T_{03} can be found by equation (2.77). The next step is to guess M_3 to obtain T_3 and v_3. Assuming that $A_3 = A_1 + A_2$, one can use continuity to find the pressure according to the following expression.

$$P_3 = \frac{\dot{m}_3 R_3 T_3}{v_3 A_3} \tag{2.83}$$

All terms are now known to compute the momentum balance from equation (2.81). The resulting Mach number is reiterated until convergence is reached with the momentum balance.

When the two fluids mix, there will be a small pressure drop due to the interaction between the streams and a pressure ratio close to unity could be assumed.

2.3.5 Water recovery

The water recovery step is crucial for making the engine concept operational. There are several ways of collecting the water that is condensed out of the hot flue gases.

It is convenient to perform most of the condensation in the condenser due to the lower velocities through the plates, thus resulting in a higher residence time and making the water recovery easier. The condensation of water in the flue gases will create droplets or a water film along the condenser plate wall which will locally increase the heat transfer coefficient [1]. The condensing water should be collected immediately and should not enter the subsequent components as the droplets might cause corrosion on the cold turbine blades or complicate the mixer process.

The collection of water in the mixer step is more difficult. The high velocity in the mixer makes the blow out of water a considerable risk due to the low residence time. Normally, if a system is in constant equilibrium, water droplets will start to form as soon as the temperature is lowered below the dew-point but due to the extreme conditions it is hard to predict how, where and at what rate the droplets will form [1]. For the practical extraction of water in a free flow, centrifugal separator units can be used. The condensation process is dependent on the availability of surrounding surfaces, one alternative could be to use angled plates which are placed along the direction of travel. These plates will provide surface for the condensation to occur and as they are angled, they will create better contact between the flow and the surface. The process of recovering water will induce losses which will affect the pressure. This can be accounted for by assuming a loss factor.

2.4 Physical properties

In this section, details about the estimation of physical properties will be accounted for.

2.4.1 Water properties

All water and steam properties necessary for calculations, such as enthalpies, heat capacity viscosity etc, were gathered by using a computer macro application called XSteam. The program is of an industrial standard, IAPWS IF-97, and is an open access program which can be found online [33].

2.4.2 Heat capacity

Heat capacity is an important variable and thus it is important to use correct expressions to get more accurate result. The formula for the heat capacity of air is shown in equation (2.84) and was supplied by the thesis supervisor [34]:

$$C_{P,air} = 961 + 0.123T + 8.2 \cdot 10^{-5}T^2 - 3.5 \cdot 10^{-8}T^3 \tag{2.84}$$

The heat capacity for flue gases can be determined from a similar expression and is shown in equation (2.85). The expression was also supplied by the thesis supervisor [34],

$$C_{P,air} = 961 + 0.123T + 8.2 \cdot 10^{-5}T^2 - 3.5 \cdot 10^{-8}T^3 + 2200FAR \tag{2.85}$$

where FAR is the fuel to air ratio which can be computed according to equation (2.86).

$$FAR = \frac{m_{fuel}}{m_{air}} \tag{2.86}$$

The heat capacity for steam can be estimated by using equation (2.87) which is valid in the interval of 338.15K - 450K.

$$\begin{aligned} C_{p,steam} = 2.95137 - 2.75514 \cdot 10^{-2}T + 2.8479 \cdot 10^{-4}T^2 \\ - 1.32088 \cdot 10^{-6}T^3 + 2.31699 \cdot 10^{-9}T^4 \end{aligned} \tag{2.87}$$

and equation (2.88) which is valid in the interval of 450K - 1700K.

$$\begin{aligned} C_{p,steam} = {} & 1.74507 + 2.04207 \cdot 10^{-4}T + 5.1756 \cdot 10^{-7}T^2 \\ & - 1.79631 \cdot 10^{-2}T^3 \end{aligned} \tag{2.88}$$

When steam is injected and mixed with the flue gases, the heat capacity will alter. The steam and flue gas mixture heat capacity is calculated according to equation (2.89) [35]:

$$C_{p,mixture} = w_{steam}C_{p,steam} + w_{fluegas}C_{p,fluegas} \tag{2.89}$$

The ratio of heat capacities, λ, can be found according to equation (2.90):

$$\lambda = \frac{C_p}{C_V} = \frac{C_p}{C_p - R} \tag{2.90}$$

If the heat capacities are on a mass basis, the gas constant, R, is the specific gas constant, and can be calculated with equation (2.91),

$$R_{specific} = \frac{R_{Universal}}{M_{mixture}} \tag{2.91}$$

where $M_{mixture}$ is the mixture molar mass and $R_{Universal}$ is 8.3143 J$K^{-1}mol^{-1}$ [26]. The mixture molar mass can be computed by performing a chemical balance of the species within the mixture. When accounting for the combustion in the combustion chamber, one can assume a mean fuel molecule of CH_2.

2.4.3 Vapor pressure

Vapor pressure is an important concept for all condensation occurring in this work and it is temperature dependent. When the mixture has reached its saturation point, or if it is oversaturated, steam will start to condense out of the mixture. The vapor pressure is a measure of the maximal amount of water vapour that can potentially exist above liquid water in the surrounding atmosphere. The common term for this is the relative humidity and is defined as the following [36],

$$RH = \frac{P_{Partial}}{P^*(T)} \tag{2.92}$$

where RH is the relative humidity, $P_{Partial}$ is the partial pressure of water vapor in air and P^* is the vapor pressure, which has a temperature dependency. In normal circumstances the relative humidity can have a maximum value of unity, as a higher value would mean that air is supersaturated, but during extreme conditions local temporal clusters of supersaturated air can be present [1]. For the estimation of vapor pressure, P^*, the work of Arden L. Buck [18] has been used in this work. Buck's equations for vapor pressure are easily implemented on a computer program for calculations and are very accurate in the range of -80^oC to +50^oC [18]. Buck's method also contains an enhancement correction factor that is used when calculating the vapor pressure in moist air as it will differ compared to pure water vapor.

Equation (2.93) is used to determine the vapor pressure of water above 0 ^oC and equation (2.94) is used to calculate the vapor pressure below 0 ^oC.

$$P_w^* = 6.1121\Big(1.0007 + 3.46 \cdot 10^{-6} P\Big) exp\Big(\frac{17.502 \cdot T}{240.97 + T}\Big) \tag{2.93}$$

$$P_i^* = 6.1115\Big(1.0003 + 4.18 \cdot 10^{-6} P\Big) exp\Big(\frac{22.452 \cdot T}{272.55 + T}\Big) \tag{2.94}$$

where the equations require both pressure, P (millibar), and temperature, T (^oC) as input. The cooling air that is used to condense water in the final stage of mixing contains some water vapor in the form of vapor pressure. It is to be noted that at a cruise altitude of over 10 000 m, the temperature is so low that the vapor pressure is very small.

2.4.4 Viscosity

Viscosity for O_2, N_2, CO_2 and water vapor was found in an online databank, Engineering Toolbox [37], for different temperatures. A curve fitting was performed on the available data points and a mean viscosity was calculated as in equation (2.95) with correct molar fractions where needed,

$$\mu_{mixture} = x_{O_2}\mu_{O_2} + x_{N_2}\mu_{N_2} + x_{CO_2}\mu_{CO_2} + x_{vapor}\mu_{vapor} \tag{2.95}$$

where the component viscosity is described by a linear equation of the same shape as equation (2.96),

$$\mu_i = a_i T + b_i \tag{2.96}$$

where the coefficients are shown in Table 2.1.

Table 2.1: Coefficients a and b in equation (2.96) for viscosity calculations.

Specie	a	b
N_2	3.62E-8	1.73E-5
O_2	4.40E-8	1.99E-5
CO_2	4.10E-8	1.43E-5
H_2O	3.97E-8	8.57E-6

3
Methods

Within the given limitations, the implementation and evaluation of the WET cycle concept is very complicated due to the large number of degrees of freedom. The methodology for this thesis is a combination of qualified assumptions and a heuristic approach to design the three main parts of the WET cycle: ***(i)*** Modifying the general turbofan cycle for the WET cycle implementation, ***(ii)*** designing the HRSG, ***(iii)*** designing the condenser and mixer. A thorough literature study was performed with the purpose of finding acceptable correlations for the design procedure of the HRSG and the condenser.

3.1 General cycle

The general engine cycle was created by the thesis supervisor prior to the thesis start and was given to the group when the work began. The group performed calibration of the model using data created by the gas turbine performance tool GESTPAN. The data was provided by a PhD student (Oliver Sjögren) [38] at Chalmers University of Technology. The method of calibration was performed by varying different factors until key parameters, such as temperature and pressure, at the different stations in Figure 2.1 were in alignment with the provided data. The varied parameters were:

- Compressor isentropic efficiency
- Turbine isentropic efficiency
- Combustion temperature
- Nozzle efficiency

The engine mass flow, bypass ratio and compressor bleed were also a part of the acquired data. Since it was not part of the original template, blade cooling had to be added to the calculations.

The cycle is considered to be operated at max cruise operation at an altitude of 35000 feet, where ambient parameters are gathered from International Standard Atmosphere in literature [10] and a cruise Mach number of 0.85 is considered.

3.1.1 WET cycle

With the use of steam injection, physical properties change in the cycle which had to be accounted for. It is accounted for by using mass and molar balances, as described in the theory section 2.4, and modifying the following parameters:

- Mixture heat capacity

- Mixture heat capacity ratio

The most available data from the proposed article [1] was when using a water to air ratio of 40%. As this operating condition contained most results, this master thesis is based on that operational condition. The following results were implemented in this work:

- Overall pressure ratio (OPR) of 30
- Core mass flow reduction of 61%

The reduced amount of core flow is moved to the bypass flow after the fan. Any additional propelling nozzle in the WET cycle is assumed to have an isentropic efficiency of 99%.

3.2 Heat Recovery Steam Generator

The method for designing the HRSG is an iterative process where an initial guess is made for the overall heat transfer coefficient. The heat transfer area is then found with equation (2.24) which is required for solving the equations described in the theory section of the HRSG. When the heat transfer coefficient has been calculated with the correlations given in the theory section, the overall heat transfer coefficient is calculated with equation (2.25). The iteration process continues until convergence is found. Fouling was not predicted to be of great importance, and therefore not investigated, so the terms involving the dirt coefficients were therefore neglected in equation (2.25). The correct area is found with the iterated overall heat transfer coefficient, which is needed for calculating the pressure drop.

The tubes used in the HRSG were chosen as small as possible since the ratio of the area to the volume increases with decreasing tube radius. The minimum theoretical tube thickness could be calculated with Barlow's formula, equation (2.28), but in this work a higher tube thickness was chosen in order to have a safety margin. The tubes are to be made of a nickle-based alloy, as was proposed in the article by MTU [1], due to the high temperature. The final tube diameter and tube thickness was chosen after investigating available tube sizes by producers such as Sandvik.

The HRSG is conically shaped and located in the nacelle directly after the LPT as stated in the article [1]. In a conventional turbofan engine, the core flow and the bypass flow exits at the end of the nacelle, but in the WET cycle implementation only the bypass flow exits at the end of the nacelle. In the WET cycle the core flow heat exchanges with the water in the HRSG and then flows towards the condenser through the wing. The water coming from the reservoir enters the tube rows located farthest away radially from the centre and then flows inwards in the tubes which are wired as a spiral around the axial line in the nacelle. The HRSG is designed so that the water in the tubes has been evaporated and superheated to the desired temperature by the time it has reached the innermost tubes in the radial direction. The innermost tubes in the radial direction are then interconnected and the water is injected into the combustion chamber. In Figure 3.1 it is seen how the flue gases, illustrated as orange arrows, exit the LPT from the right and flow radially toward the HRSG, where station 1 is the inlet and station 2 is the outlet.

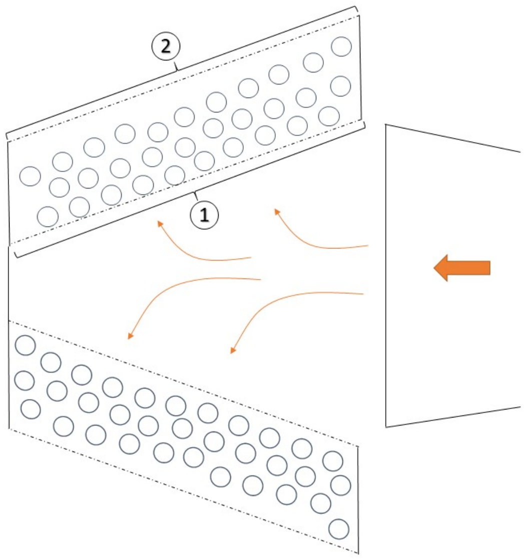

Figure 3.1: Cross-sectional picture of the HRSG.

3.3 Water recovery system

3.3.1 Plate heat exchanger

The plate heat exchanger is located in the main body of the aircraft as suggested in the article [1]. The design process of the plate heat exchanger is an iterative procedure. When designing the plate heat exchanger, the allowable pressure drop is an important parameter as it will dictate some of the design parameters. It is set as the minimum pressure entry level for the turbine and the exit pressure level of the HRSG. Three different plate heat exchanger designs were investigated, 1-pass/1-pass crossflow, 1-pass/2-pass crossflow and a counter current heat exchanger. See Figure 3.2 for an illustrative representation of the heat exchangers.

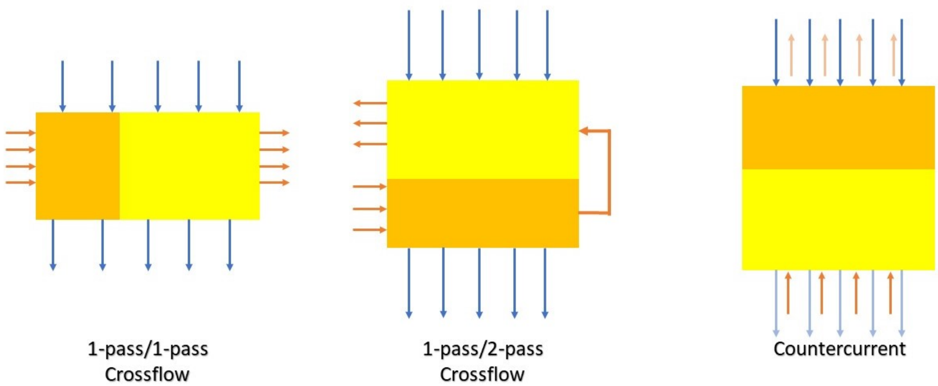

Figure 3.2: Illustrative representations of the investigated condenser heat exchangers. Orange part represents cooling of hot flue gases, yellow part represents condensing part of the flue gases.

The three different architectures have different limits on possible inlet and outlet temperature conditions which consequently affect the required cold air mass flow. The table below shows what conditions are used to estimate the outlet temperatures for the different designs. For the crossflow heat exchangers, efficiency needs to be accounted for and the efficiency will depend on which fluid is considered mixed and which fluid is considered unmixed. The interpretation of mixed and unmixed in this work is whether the temperature can be considered constant in a certain direction along the heat exchanger, if so it is considered mixed, and if not, it is considered unmixed. Looking at the 1-pass/1-pass in Figure 3.2, the temperature of the cold air can not be assumed to be constant in any vertical or horizontal segment. While in the counter current flow, the temperature of any fluid along any horizontal segment can be considered constant, but the temperature will change in the vertical direction. In crossflow, it is expected that there will be temperature difference in all directions and will thus yield an unmixed-unmixed configuration. Due the lack of efficiency estimation equations for unmixed-unmixed streams, the fluid undergoing the lowest temperature change is considered mixed while the fluid undergoing the highest temperature change is considered unmixed, as there is more room for temperature variations at the exit. Considering the condensing step, the temperature difference between the flue gas inlet and outlet will be small and thus difference between the hottest and coldest outlet will not be very large compared to the cold air that is cooling the condensing step.

Table 3.1: Temperature parameters used for calculations in the cooling section of the plate heat exchanger.

Architecture	$T_{H,in}$ **[K]**	$T_{H,out}$ **[K]**	$T_{c,in}$ **[K]**	$T_{c,out}$ **[K]**
1/1 - Pass	$T_{HRSG,exit}$	$T_{condense,start}$	$T_{fan,inlet}$	$T_{condense,start}$ - dT_{pinch}
1/2 - Pass	$T_{HRSG,exit}$	$T_{condense,start}$	$T_{condense,end}$ - dT_{pinch}	$T_{condense,start} + \Delta T_{increase}$
Countercurrent	$T_{HRSG,exit}$	$T_{condense,start}$	$T_{condense,start}$ - dT_{pinch}	$T_{c,in} + \Delta T_{increase}$

Table 3.2: Temperature parameters used for calculations in the condensing section of the plate heat exchanger

Architecture	$T_{H,in}$ **[K]**	$T_{H,out}$ **[K]**	$T_{c,in}$ **[K]**	$T_{c,out}$ **[K]**
1/1 - Pass	$T_{condense,start}$	$T_{condense,end}$	$T_{fan,inlet}$	$T_{condense,end}$ - dT_{pinch}
1/2 - Pass	$T_{condense,start}$	$T_{condense,end}$	$T_{fan,inlet}$	$T_{condense,end}$ - dT_{pinch}
Countercurrent	$T_{condense,start}$	$T_{condense,end}$	$T_{fan,inlet}$	$T_{condense,start}$ - dT_{pinch}

For the crossflow heat exchangers, $\Delta T_{pinch} = 10$ K is chosen due to the uneven temperature distribution. This value is thought of representing the mean temperature difference at the pinch point. While the counter current heat exchangers are investigated with a $\Delta T_{pinch} = 5$ K and $\Delta T_{pinch} = 10$ K.

The $\Delta T_{increase}$ is the temperature increase due to the excess of energy from the second heat exchanging stream, i.e. the due to the duty that needs to be transferred.

By altering the gap between the plates, the velocity can be controlled and consequently the pressure drop. A higher gap would then correspond to a lower velocity which results in a lower pressure drop. However, it also results in a decrease of the heat transfer, so an iterative procedure is required to find a satisfying plate gap distance.

All plate heat exchanger architectures were designed for a high heat transfer coefficient to reduce weight, but this comes with the cost of a higher pressure loss. For comparison, the counter current heat exchangers were also designed for a low-pressure loss on the cold side.

3.3.2 Cold Turbine

No detailed studies of the cold turbine were performed. A pressure ratio of 1.5 is set for the cold turbine and an isentropic efficiency of 95 %.

3.3.3 Secondary fan and duct inlet

No detailed studies were performed on the secondary fan and the pressure ratio over the fan is varied until the work required by the fan equals the work produced by the cold turbine. An isentropic efficiency of 98 % is assumed for the fan and a pressure ratio of 99.8 % for the duct intake.

3.3.4 Mixer

In the mixer part, it is important to distinguish between two possible extremes for the condensation process in the mixer section. One extreme is that the entering cold air is deaccelerated and the second scenario is that the velocity of cold air remains unaffected by the entry to the secondary duct. When designing the mixer zone, the velocity of cold air can take any value between these two extremes, including the extreme values.

In the first extreme scenario, if cold air is decelerated and mixes with the flue gases with a significantly lower velocity (than cruise velocity), the inlet temperature of the cold air will be significantly higher. This is because that the flow will, in relative terms, become stagnant and temperature will rise. This will result in a lower difference between cold fluid inlet and outlet temperature after mixing ambient air with the flue gases in the mixer section. The temperature difference drives the heat exchanging process and when it decreases, more air is required which further dilutes the resulting mixture. This scenario has some benefits of increasing the residence time in the mixer which might aid the condensation and recovery process. The risk of blowing out the steam is also considerably lower as the velocities are lower. There is also the benefit of friction forces being lower on the internal structure.

In the second scenario the flow of cold air will enter the secondary air duct and pass through it with the same velocity as the aircraft. If air is to pass through the duct with such high velocity, complications can occur. The friction exerted to the duct walls will be high and there will be a high demand for a simple architecture within the duct as the cold air flow is not to be significantly disturbed as this might then cause component wear and tear. The benefit of using this type of architecture is that the cold air is not stagnant, in relative terms, and a higher temperature difference can be achieved between the flue gases and the cold air. This is beneficial as a smaller amount of air is then needed, and as the condensation process is vapor pressure dependent, it will be increasingly feasible to condense the steam.

When performing calculations, the hot exhaust temperature out of the cold turbine is held constant while the cold air is conceptually thought of retaining the condensation energy and thus rising in temperature until it has reached the same temperature as the hot stream. After the energy exchanging process, the two flows are mixed, and a resulting temperature is reached. Prior to the mixture leaving the system, it will pass through a water recovery unit where the water droplets are collected and reused by the system. For clarification of this procedure, see Figure 3.3.

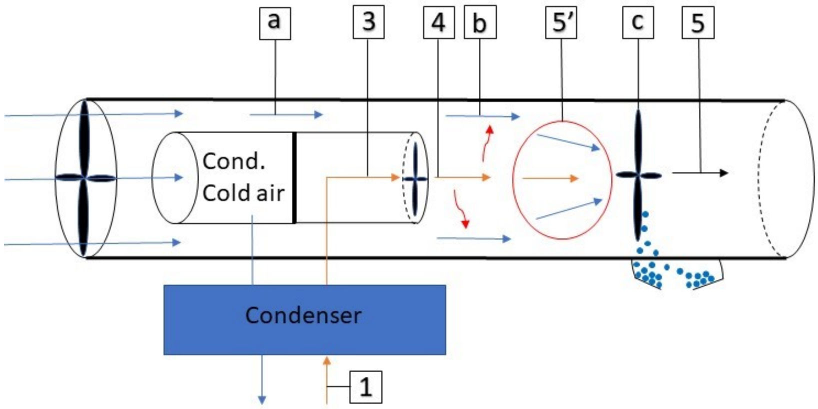

Figure 3.3: Illustrative representations of the used procedure for calculations when mixing.

In Figure 3.3, the same notations apply as in Figure 2.3 but with the addition of three points ($a/b/c$). Flue gases have the color code orange while cooling air is blue.

Station 1 represents the flue gas inlet into the condenser, which also is the HRSG outlet. After heat exchanging in the condenser, the now cooler flue gases will exit the condenser and head towards the cold turbine (station 3). The flue gases will pass the cold turbine and expand, lowering both temperature and pressure (station 4). Cold air entering the system will either be sent towards the condenser or bypassed and sent towards the mixer section, the bypassed air is denoted as station a. As was mentioned previously, depending on the velocity of the cold air in the mixer duct, which is determined by the designer, the static temperature will differ, consequently affecting the heat exchange. The cooler air will absorb the condensing heat of the flue gases before they are mixed, this happens in station b. It is to be noted that this is not what happens in reality, but is a result of the splitting of the physical processes occurring in the mixer section. The cold air and flue gases will mix, and if no condensation would occur station 5' would be reached. But as condensation is occurring, the water droplets are gathered by the water recovery unit, station c, and a stream with less water is produced, station 5. The collected water is sent back towards the system, either to a reservoir or the HRSG, and the mixture stream (air and exhaust gas) will be ejected out of the system via a nozzle.

The procedure chosen is one of several possible scenarios and it is all based on the fact that it is unpredictable to estimate the real process exactly. It is likely that a fraction of the hot flue gases starts to self-condense prior to the addition of air which means that the flue gas temperature will rise, and not be held constant as has been assumed in our calculations. It is however not possible to estimate to what extent the condensation will occur during the brief time after the cold turbine, and prior to the air addition, and thus it is hard to perform calculations with this approach. The chosen procedure is not optimal, but it will highlight some important factors in the mixer process.

Due to the lack of enthalpy data for water/steam below 0^oC, it is hard to estimate a proper heat of condensation for the process. For all condensation that occur below 0^oC, the enthalpy difference between saturated vapor and liquid at 0^oC is assumed to be the heat of condensation. It should be noted that a small error is induced due to this approach.

The water recovery unit, after the mixer, were not investigated in any detail, but a pressure ratio of 0.97 was set to account for potential losses due to the recovery of water.

4

Results

Results are presented for max cruise conditions and are to some extent compared with the results presented in the articles by Schmitz et al [1] [2]. The WET cycle is based on data for a GEnx-1B engine and has not been thoroughly optimized for each investigated case, as it was not the aim of the project.

4.1 Reference cycle

The results for the reference cycle are based on the data provided by Oliver Sjögren [38] for a conventional, simple cycle, turbofan. Various important parameters for the reference cycle are presented for comparison with the results from the WET cycle implementation in Table 4.1.

Table 4.1: Main GEnx data at max cruise conditions.

Inlet flow [kg/s]	505	Fuel Flow [kg/s]	1.03
Bypass flow [kg/s]	453.12	Compressor exit flow [kg/s]	51.86
BPR	8.74	Combustor inlet flow	37.86
Thrust [N]	64409	Turbine inlet flow [kg/s]	45.89
SFC [mg/(N s)]	15.9	Cooling flow [kg/s]	14.00
OPR	48.6	Turbine inlet pressure [bar]	18.00

The dataset provided by Oliver Sjögren originates from a thermodynamic cycle model based on open published data from the manufacturer. All mass flows, the BPR and OPR were adapted to the reference cycle in accordance with the provided dataset. The fuel flow, thrust, SFC and turbine inlet pressure was acquired by altering component isentropic efficiencies in the reference cycle until close alignment with the dataset was found. The difference between compressor exit flow and combustor inlet flow is the cooling bleed, and it was set to 27% of the compressor exit flow in accordance with provided dataset. The turbine inlet flow is the sum of combustor inlet flow, the fuel flow and 50% of the cooling bleed. The acquired isentropic efficiencies are presented in the table below.

Table 4.2: Modelled GEnx cycle component efficiencies.

Component	η_{is}
Outer Fan	0.88
Inner Fan	0.90
Low pressure compressor	0.86
High pressure compressor	0.85
High pressure turbine	0.90
Low pressure turbine	0.92

4.2 The WET cycle

The WET cycle in this study builds on the GEnx cycle. Several assumptions such as OPR and core mass flow reduction are based on the results from the article made by Schmitz et al [1]. These assumptions have been merged with the dataset provided by Oliver Sjögren [38]. The pressure ratio has been equally scaled down at all compressing stages in the reference cycle, except for the main GEnx fan which remained constant, to acquire the OPR provided by Schmitz et al. The core mass flow in the reference cycle was reduced in accordance with the article to acquire a WET cycle core mass flow. The injected amount of water was chosen so that a water to air ratio of 0.4 could be achieved at the combustor exit.

Several different WET cycle designs were modelled for the purpose of comparison with the reference cycle. The WET cycle general data is presented in the table below.

Table 4.3: Wet cycle general data.

Inlet flow [kg/s]	505
Bypass flow [kg/s]	483.4
BPR	22.4
Thrust [N]	Se section 4.2.4
SFC [mg/(N s]	Se section 4.2.4
OPR	30
Fuel flow [kg/s]	0.78

The BPR has increased as the core mass flow was reduced by 61 %. The thrust and SFC cannot be specified in one table and the reader is referred to the designated section as several scenarios have been investigated. The fuel flow has been reduced by 22 %, which is close to the 30 % presented by the article from MTU [1]. The bleed fraction used for cooling the high pressure turbine is the same as in the reference cycle (27 % of compressor exit flow). Steam has also been introduced to the cycle now. In Figure 4.1 some key points have been marked and the temperature, pressure and mass flow properties are given in Table 4.4. Note that not all stations can be provided with a single value as several cases are investigated.

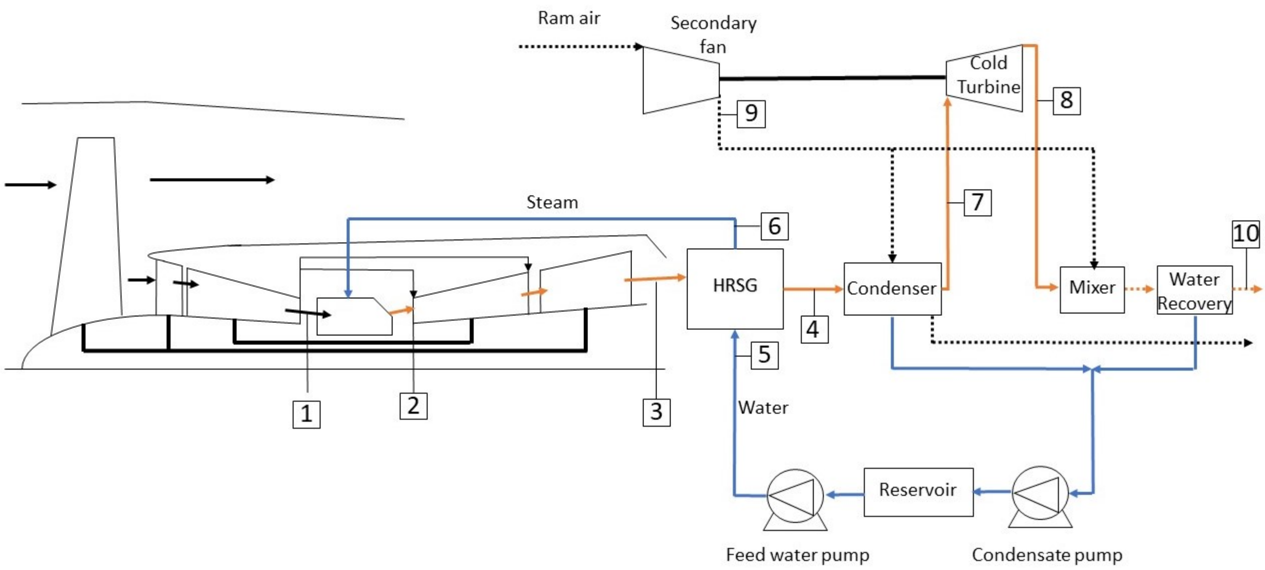

Figure 4.1: WET cycle depiction with station markings.

Table 4.4: Accompanying table for Figure 4.1 with station properties for the WET cycle.

Station	Total temperature [K]	Total pressure [kPa]	$\dot{m}$ [kg/s]
1	727	1110	15.75
Compressor bleed	727	1110	5.83
2	1650	1110	24.66
3	980	72.17	27.57
4	531	66.14	27.57
5	293	1110$^{(1)}$	5.21
6	923	1110$^{(1)}$	5.21
7	See Appendix A.4	59.94	27.57
8	See Appendix A.14$^{(2)}$	39.96$^{(3)}$	27.57
9	See Appendix A.10	See Appendix A.11	See Appendix A.10
10	See Appendix A.17	See Appendix A.18	$\dot{m}_{Coldturbine} + \dot{m}_{air}$ $^{(4)}$

1 Due to pressure losses, the real pressure will be higher.
2 Small deviations exist due to the mixing, refer to Table Appendix A.12.
3 Static temperatures deviates due to different velocities in mixer section.
4 $\dot{m}_{air}$ is found in Appendix Table A.5

One important result is that 1.00 kg/s water is created in the combustion, and 5.21 kg/s water is injected into the combustion chamber. All together, the water constitutes 22.5 % of the mass fraction at station 3 in Figure 4.1.

The power of the secondary fan was approximately 870 kW, which was 5 % relative the main engine fan, and it caused 2 - 5 % pressure rise depending on the amount of cooling air passing through it (see Appendix section A.3).

4.2.1 Heat Recovery Steam Generator

The HRSG was designed according to the assumptions and choices presented in the method section. The used equations are written in the theory section. Refer to Figure 3.1 for a depiction of the HRSG design. The results from the sizing of the HRSG, with the procedure described in the theory, and weight is shown in the table below. The area is the total inner heat transfer area which is required, and is consequently divided shared by all installed tubes.

Table 4.5: HRSG dimensions and weight.

Area Eco [m^2]	Area Evap [m^2]	Area Sup [m^2]	Area tot [m^2]	Weight [kg]
60	123	122	305	627

The tubes in the HRSG are made of Inconel 625, which is a nickel-based superalloy, due to the high temperature of the flue gas. The inner diameter of the tubes was set to 10 mm and the tube thickness was set to 0.25 mm. The tube thickness was estimated by calculating the rupture pressure from internal tensions from data for the material and system specifications such as working pressure. The tube thickness could have been set to approximately 0.1 mm, but was set to 0.25 mm in order to have a safety margin.

With the mass-continuity balance the velocity of the flue gas through the HRSG tube banks was calculated. The cone shape of the HRSG results in a higher inlet velocity to the tube bank than the outlet velocity of the tube bank. The flue gases flows radially outwards, with an increasing cross sectional area, which results in a decrease of the velocity (see Appendix Figure A.1). Therefore, an averaged velocity is presented in the table below and it is used to calculate the pressure drop over the tube bundle for the flue gas. The velocity for water in the tube side is a mean between economizer inlet and outlet, and the velocity for steam in the tube side is a mean between superheater inlet and outlet. The increase in velocity for steam is due to expansion as water evaporates.

Table 4.6: Fluid velocity and pressure drop in the HRSG.

	Mean velocity [m/s]	ΔP [kPa]
Flue gas	48.0	4.952
Tube d_i = 10 mm (water)	0.65	20.333
Tube d_i = 10 mm (steam)	167	4467
Tube d_i = 15 mm (steam)	74.1	567.3

With an inner diameter of 10 mm for the tubes, the pressure drop for the steam side is significant and even higher than the operating pressure for the combustion chamber. A pressure drop that is 4-5 times higher than the operating pressure is not deemed practical. For these reasons, a diameter of 15 mm was tried and the results show a lower pressure drop, as expected, and the pressure drop falls below the operating pressure. This result shows that the inlet diameter of the tubes on the steam side should be higher than on the water side to lower the pressure drop.

4.2.2 Condenser

Three different plate heat exchanger designs were investigated with varying degree of condensation in the plate heat exchanger. All plate heat exchangers are designed with plates of 8 m^2 and a plate thickness of 0.3 mm. The designs differ from each other by the amount of injected water that is condensed in the plate heat exchanger and in the mixer. The case with 75 % is the case where 75 % of the injected water is condensed in the plate heat exchanger and the remaining 25 % of the injected water is condensed and separated in the mixer.

In Tables 4.7 and 4.8, the results from the dimensioning of the plate heat exchangers are shown for comparison between different architectures. It contains information for three different types of architectures when condensing 75 % of the injected steam. Note that the counter current architecture is investigated with two different pinch point temperatures. The design procedure was conducted as to maximize the overall heat transfer coefficient for the comparison of different architectures. The designs were sought to have equal pressure drops on both sides.

Table 4.7: Plate heat exchanger results for the investigated configurations when condensing 75 % of the injected steam and designing for higher heat transfer.

Configuration - Higher U	$\dot{m}_{air,PHX}$ [kg/s]	Weight [kg]	ΔP (Exhaust/Air) [Pa]
1-pass/1-pass Crossflow	278.62	2579	6126/10821
1-pass/2-pass Crossflow	176.01	3331	6197/9545
Countercurrent ΔT_{pinch} = 10K	137.54	3700	6195/9761
Countercurrent ΔT_{pinch} = 5K	128.19	4731	6110/10104

Table 4.8: Total plate area and volume of plate heat exchangers when condensing 75 % of the injected steam and having higher heat transfer.

Configuration - Higher U	Total plate area [m^2]	Volume of plate heat exchanger [m^3]
1-pass/1-pass Crossflow	3182	49.1
1-pass/2-pass Crossflow	4105	74.3
Countercurrent ΔT_{pinch} = 10K	4565	47.4
Countercurrent ΔT_{pinch} = 5K	5827	51.4

As can be seen in the 75% case in Tables 4.7 and 4.8, the 1-pass/1-pass architecture is the lightest and smallest structure, and this feature can be attributed to the higher ΔT_{lm} achieved in its design between the streams. However, it suffers from large cooling air flows. The 1-pass/2-pass is still lighter than the countercurrent design and requires less cooling air than the 1-pass/1-pass crossflow heat exchanger as it also has slightly higher ΔT. The 1-pass/2-pass is however larger than the other cases, which is a disadvantage. The counter current design with a ΔT_{pinch} of 5K is heavier than the countercurrent design with a ΔT_{pinch} of 10K, but the first mentioned has a slightly lower cooling air requirement. The higher weight for the ΔT_{pinch} of 5K is attributed to the lower approach temperature that is reached. All of these designs have a high cold side pressure drop due to the higher overall heat transfer coefficient.

Table 4.9 shows results for six different countercurrent plate heat exchanger designs, where they differ in the amount of condensed injected water. The cases investigated are 50-/75-/100 % condensation of the injected water in the plate heat exchanger. Each case has one heat exchanger that is designed for a higher overall heat transfer coefficient and one that is designed for a lower pressure drop in the cold side.

Table 4.9: Plate heat exchanger design results for all three cases with either higher heat transfer or lower pressure drop for cold side with $\Delta T_{pinch} = 5$K.

Configuration - Higher U	$\dot{m}_{air,PHX}$ [kg/s]	Weight [kg]	ΔP (Exhaust/Air) [Pa]
Countercurrent 50%	84	3674	6141/11634
Countercurrent 75%	128	4731	6110/10104
Countercurrent 100%	176	6545	6034/11750
Configuration - Lower ΔP_c	$\dot{m}_{air,PHX}$ [kg/s]	Weight [kg]	ΔP (Exhaust/Air) [Pa]
Countercurrent 50%	84	4154	6135/4290
Countercurrent 75%	128	5579	6121/4912
Countercurrent 100%	176	7459	6139/4635

From Table 4.9 it can be seen that by allowing a higher pressure drop, the weight can be reduced. However by allowing a higher weight for the plate heat exchangers, the pressure drop on the cold side can be significantly reduced.

Table 4.10: Total plate areas and volume for all three cases with either a higher heat transfer or lower pressure drop for cold side with $\Delta T_{pinch} = 5$K.

Configuration - Higher U	Total plate area [m^2]	Volume of plate heat exchanger [m^3]
Countercurrent 50%	2265	37.8
Countercurrent 75%	2914	51.4
Countercurrent 100%	4036	63.5
Configuration - Lower ΔP_c	Total plate area [m^2]	Volume of plate heat exchanger [m^3]
Countercurrent 50%	2558	50.7
Countercurrent 75%	3220	67.6
Countercurrent 100%	4602	86.9

The design data used for generating the results is shown in Appendix Table A.5 - A.9.

From table 4.10, one can see that the size of the heat exchangers with a higher heat transfer is significantly smaller than the other case. However, a larger heat exchanger might be required due to the higher outlet cold side pressure, as this is a significant factor in generating thrust.

One result already shown in Figure 2.2 is that the condenser cooling air is ejected after the heat exchange in the condenser. This was found to be the better solution as this would avoid the addition of unnecessary heat into the mixer section. This additional heat would require a larger cooling air intake which would only impair the extraction process in the mixer.

4.2.3 Mixer

As has been stated earlier, the naming of the cases is the percentage of how much of the injected steam is condensed in the condenser. The investigated cases were 50 %, 75 % and 100 %. For each of these cases, three different Mach numbers of the cooling air through the mixer duct have been tested and these were 0.25, 0.5 and 0.85. For the readers convenience, Figure 3.3 is shown again below.

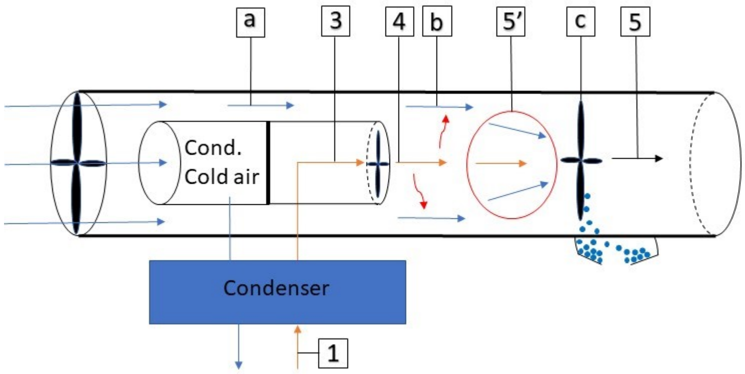

Table 4.11 shows the calculated data on water extraction in the mixer section for the different cases. The first and second column in table 4.11 shows what condenser case is applied (% of injected water recovered in the condenser), and the investigated cold air velocity. $\dot{m}_{water}$ is the amount of water left in the flue gases entering the mixer section and the fourth column shows the aimed for extraction amount. The results shown is selected data on the minimal requirements and for the maximal possible extraction. The minimal requirement is the recovery of the remaining injected water. The maximal possible extraction is the amount of created water that is extractable, which is when a RH = 1 is achieved at the exhaust (station 5 in the figure above). This limit indicates whether the solution is undersaturated or oversaturated. A solution below RH = 1 is undersaturated, meaning that the aimed extraction can not be attained. It is important to understand that the 'aimed for' extraction amount is a trial and error procedure, where different degrees of extractions are tried and the resulting RH value is observed, and whenever a RH = 1 is achieved the maximum recoverable amount has been found. The term 'injected' refers to the water that has been injected into the combustion chamber, which corresponds to the amount of water that needs to be recovered in order for the cycle to be self sufficient. The 'created' refers to the created water from combustion. When extracting created water, the cycle is then actively lowering engine water emissions into the atmosphere. In the 75 % case, 75 % of the injected water is recovered in the condenser while the remaining 25 % of the injected water plus potentially additional created water is recovered in the mixer. For total amounts of water refer to table 4.4. The $\dot{m}_{air}$ is the required mass flow of air to the mixer section. The last column shows the relative humidity at the exhaust for the attained solution.

Table 4.11: Mixer extraction results for different cases. Station designation for supporting figure is in parenthesis.

Case	$M_{air(a)}$	$\dot{m}_{water(4)}$ [kg/s]	$\dot{m}_{water,extracted}$ [kg/s] (Injected/Created)	$\dot{m}_{air(a)}$ [kg/s]	$RH_{(5)}$
50%	0.25	3.61	2.61 / 0	215.73	0.263
50%	0.5	3.61	2.61 / 0	225.97	0.424
50%	0.85	3.61	2.61 / 0	244.73	0.988
75%	0.25	2.30	1.30 / 0	135.77	0.592
75%	0.5	2.30	1.30 / 0	140.67	1.000
75%	0.85	2.30	1.30 / 0	152.08	2.093
75%	0.85	2.30	1.30 / 0.48	215.20	1.020
100%	0.25	1.00	0 / 0.10	20.19	4.546
100%	0.25	1.00	0 / 0.49	99.43	1.028
100%	0.5	1.00	0 / 0.10	20.88	9.945
100%	0.5	1.00	0 / 0.68	142.94	1.029
100%	0.85	1.00	0 / 0.10	22.60	60.551
100%	0.85	1.00	0 / 0.93	212.09	1.060

The 50 % case with a Mach number of 0.25 for the cold air at the inlet to the mixer, 3.61 kg/s of water is left in the flue gases after the condenser. In order to recover a sufficient amount of water for the WET cycle, 2.61 kg/s of the water needs to be recovered. To perform this, 215.73 kg/s cold air is required in the mixer. However, this produces a solution with a RH of 0.263 (station 5 in supporting figure), which indicates that the solution is undersaturated and thus it is not possible to extract a sufficient quantity of water. The same situation applies for the other 50 % cases, except for possibly when using a Mach number of slightly higher than 0.85 for the cold air at the inlet of the mixer, as this solution is closest to a RH of 1. The 75 % case has working solutions for all velocities except for a Mach number of 0.25, while the 100 % case is the most promising scenario with the lowest air flow requirements for the mixer section. However, to condense 100 % of the injected water in the condenser requires a large and heavy plate heat exchanger as can be seen in Table 4.9. In the 75 % case, with a Mach number of 0.85, the condenser and mixer can extract all of the injected water plus an additional 48 % of the created water from the combustion process. The 100 % case can extract 49 % to 93 % of the created water at Mach numbers ranging from M = 0.25 and M = 0.85. These solutions actively decrease engine water emissions to the atmosphere.

It might seem wrong that the 75 % case with a Mach number of 0.85, where 48 % of the created water is extracted, has almost the same air requirement as the 100 % case with 93 % created water extraction, even though the amount of water extracted in the 75 % case is higher than the 100 % case. It is however expected as the 75 % case has a higher turbine outlet temperature, allowing for a higher temperature difference between the incoming cold air and the hot exhaust gases. Thus, consequently requiring less air even if the duty is higher.

4.2.4 Thrust generation and cycle performance

Table 4.12 shows properties of the cooling air in the condenser nozzle properties, for all cases of condensation and for the two design goals (designing for higher heat transfer and designing for lower cold side pressure drop).

Table 4.12: Condenser exhaust nozzle data.

Case - Higher U	$T_{0,exit,air}$ [K]	$P_{0,exit,air}$ [Pa]	$v_{exit,air}$ [m/s]	$M_{exit,air}$	Nozzle gross thrust [N]
50%	413	27100.9	170.09	0.425	14246.2
75%	385	28630.6	195.46	0.510	24909.5
100%	370	26984.5	158.27	0.418	27783.8
Case - Lower ΔP_c	$T_{0,exit,air}$ [K]	$P_{0,exit,air}$ [Pa]	$v_{exit,air}$ [m/s]	$M_{exit,air}$	Nozzle gross thrust [N]
50%	413	34445.4	286.31	0.740	23980.4
75%	385	34311.0	274.95	0.736	35039.7
100%	370	34099.6	267.36	0.730	46936.2

As can be seen from table 4.12, when restricting the cold side pressure drop, a higher thrust can be obtained. The thrust generated by the condenser exhaust nozzle increases with a higher degree of extraction in the condenser, which is expected as more heated cooling air is required to pass through the condenser. The penalty for using a higher degree case is that the plate heat exchanger increases in size and weight. The table below shows the thrust generated by the mixer exhaust nozzle for the minimal required and maximal possible extraction cases. For a complete list of results, see Appendix Table A.21.

Table 4.13: Thrust generation from mixer exhaust nozzle.

Case	$M_{air(a)}$	$\dot{m}_{extracted}$ [kg/s] (Injected/Created)	Nozzle gross thrust [N]
100%	0.25	0 / 0.10	11124.3
100%	0.25	0 / 0.49	31712.5
100%	0.5	0 / 0.10	11356.4
100%	0.5	0 / 0.68	42953.6
100%	0.85	0 / 0.10	11862.0
100%	0.85	0 / 0.93	60785.3
75%*	0.25	1.3 / 0	42738.9
75%	0.5	1.3 / 0	44743.4
75%	0.85	1.3 / 0	49629.6
75%	0.85	1.3 / 0.48	65424.4
50%*	0.25	2.61 / 0	65082.7
50%*	0.5	2.61 / 0	68866.3
50%*	0.85	2.61 / 0	75909.7

* Case has a relative humidity below 1, thus not feasible.

The trend seen in Table 4.13 is that a higher thrust is generated when the degree of condensation is lower in the condenser and more condensation occurs in the mixer.

This is attributed to the increasing amount of cooling air flow required in the mixer for extraction. The increase in thrust between 100 % and 50 % for the mixer exhaust nozzle in Table 4.13 is higher than the increase in thrust between the same cases in Table 4.12 for the condenser exhaust nozzle.

In the Table below, the total thrust generated and SFC achieved is shown for the system using plate heat exchangers with higher heat transfer. The results are a selection of the minimum requirement and maximal possible extraction. For a complete list, see Appendix Table A.22.

Table 4.14: Thrust and SFC for condenser designed for higher overall heat transfer.

Case	$M_{air(a)}$	$\dot{m}_{extracted}$ [kg/s] (Injected/Created)	Engine total net thrust [N]	SFC [mg/Ns]
100%	0.25	0 / 0.10	32862.7	23.705
100%	0.25	0 / 0.49	33478.0	23.270
100%	0.5	0 / 0.10	32920.8	23.663
100%	0.5	0 / 0.68	33754.0	23.079
100%	0.85	0 / 0.10	32992.9	23.611
100%	0.85	0 / 0.93	34157.8	22.806
75%*	0.25	1.30 / 0	44599.0	17.467
75%	0.5	1.30 / 0	45368.8	17.170
75%	0.85	1.30 / 0	47378.2	16.442
75%	0.85	1.30 / 0.48	47265.0	16.482
50%*	0.25	2.61 / 0	47136.1	16.527
50%*	0.5	2.61 / 0	48338.4	16.116
50%*	0.85	2.61 / 0	50653.8	15.379

* Case has a relative humidity below 1, thus not feasible.

The SFC is higher for the cases using a condenser with higher heat transfer. The SFC is higher for all feasible scenarios compared to the SFC acquired by the GEnx reference cycle. This result indicate that the implementation of the WET cycle is not feasible for a high heat transfer condenser, even though there exists a weight reduction.

In the table below, the total thrust generated and SFC achieved is shown for the system using plate heat exchangers with lower cold side pressure drop. The results are a selection of the minimum requirement and maximal possible extraction. For a complete list, see Appendix Table A.23.

Table 4.15: Thrust and SFC for condenser designed for lower cold side pressure drop.

Case	$M_{air(a)}$	$\dot{m}_{extracted}$ [kg/s] (Injected/Created)	Engine total net thrust [N]	SFC [mg/Ns]
100%	0.25	0 / 0.10	52015.0	14.976
100%	0.25	0 / 0.49	52630.4	14.801
100%	0.5	0 / 0.10	52073.2	14.960
100%	0.5	0 / 0.68	52906.4	14.724
100%	0.85	0 / 0.10	52145.3	14.939
100%	0.85	0 / 0.93	53310.1	14.613
75%*	0.25	1.30 / 0	54729.1	14.234
75%	0.5	1.30 / 0	55499.0	14.036
75%	0.85	1.30 / 0	57508.3	13.546
75%	0.85	1.30 / 0.48	57395.1	13.573
50%*	0.25	2.61 / 0	56870.4	13.698
50%*	0.5	2.61 / 0	58072.7	13.414
50%*	0.85	2.61 / 0	60388.1	12.900

* Case has a relative humidity below 1, thus not feasible.

When allowing a higher weight of the condenser, and consequently reducing the cold side pressure drop, the SFC falls below the reference SFC of the GEnx engine. A reduction on SFC of up to 15 % is observed for the 75 % case, using a Mach number of 0.85. It is possible that a higher SFC reduction can be obtained if a case between 50 % and 75 % is explored. The 50 % case is obviously close to the minimum required condensation in the condenser as the relative humidity is close to 1.

5

Discussions

The aims of this chapter is to discuss the results and methodology of each component. The discussion consists of interpretation of the results, uncertainties and errors and suggestion of improvements.

5.1 WET cycle

According to the results, when both engines use the same fan with identical mass flow and fan pressure ratio, the GEnx cycle produces a higher thrust. The WET cycle achieves a lower SFC if the cold side pressure drop in the condenser is minimized. These results are however not suitable for comparison since no optimisation was made for the WET cycle. The articles about the water enhanced turbofan by Schmitz et al. [1] do not state the size of the engine. One hint that is given in the first article by Schmitz et al is that the overall propulsion system weight is expected to increase by 40 % compared to the conventional propulsion system. Our results indicate a much larger increase in weight, but some solutions on how to reduce the weight are presented in the plate heat exchanger discussion section.

5.2 HRSG

The mass flows, temperature and pressure were known both inside and outside of the tubes, which resulted in fewer degrees of freedom when designing the HRSG. The largest uncertainty in the design of the HRSG is the correlation for calculating the outside heat transfer coefficient. The form of the HRSG, where the flue gas flows radially outwards, is to the authors knowledge not used in any known application. No studies or correlations were found for the special form of the HRSG so correlations over tube banks were used.

Another uncertainty is the pressure drop calculation for the evaporation which is based on the velocity increase when liquid water evaporates to steam. A very high velocity of the steam is achieved in order to maintain the mass-continuity balance inside the tubes, which leads to a very high pressure drop. Evaporation is a complicated process to predict and more research would have to be made for more accurate predictions. One possible solution to lower the pressure drop could be to increase the tube diameter in the HRSG where steam is present, which would require thicker walls there. An alternative is to increase the number of tubes, in order to lower the velocity of the steam. The two solutions would however lead to an increased weight of the HRSG since more area is needed.

5.3 Plate heat exchanger

A plate heat exchanger for the given purpose, under the given conditions, has to the authors knowledge never been used. A plate heat exchanger was chosen since it was mentioned in the article by Schmitz et al. [1]. The benefit of using a plate heat exchanger is that it can be constructed out of a lighter material, such as aluminium, due to the lower temperatures in the condenser. This is an important aspect as the purpose is to install it in an airplane. Results show that a large amount of cooling air is required, for all configurations due to the condensation. Results also show how large and heavy the plate heat exchangers would be. The pressure drop is a function of the velocity and must be kept low in order to have a higher exit pressure than the ambient pressure. A lower velocity will however lead to a lower overall heat transfer coefficient which in turn leads to more plates as more area is needed. An uncertainty in the weight calculations is the thickness of the plates, which was assumed to be 0.3 mm after looking up a typical thickness used by Alfa Laval [39]. Constructing the plate heat exchanger with thinner plates would be crucial in order to reduce its weight.

The 1-pass/1-pass crossflow heat exchanger can almost immediately be rejected due to the large cold air requirement. It is however the lightest compared to the other architectures investigated. It should be noted that the air flow required is more than half of the air flow required by the main fan (Table 4.1), and that is only when the plate heat exchanger demand is accounted for. The mixer need will further increase the total air flow requirement which will only make the secondary fan larger. Having a secondary fan of the same size as the GEnx fan is unreasonable. The 1-pass/2-pass is a great improvement considering air flow requirements compared to the 1-pass/1-pass crossflow heat exchanger, but it is however heavier.

A potentially large source of error are the calculations for the heat transfer coefficient for the condensation process. In a condenser fed with pure steam the condensation results in a very high heat transfer coefficient, but in this application the condensing steam is only a smaller part of the total flue gas flow. The heat transfer coefficient was therefore calculated with correlations for non-condensing dry flow across plates, which probably resulted in calculations with a too low heat transfer coefficient. Predicting partial condensation accurately in a binary mixture, if steam and air can be treated as separate, is hard and was not the aim of this work. An interesting idea would be the usage of hydrophilic plates in order to improve contact between the water droplets and the plates. Another potential improvement could be to use a plate and fin heat exchanger in order to maximize contact area between the flowing gas and the plates. A plate and fin heat exchanger would however result in a higher pressure drop.

5.4 Mixer

The mixer is the most difficult part of the system to model, which is also stated in the articles by Schmitz et al [1]. A thorough study would have to be carried out on the condensation process in such specific conditions. The main problem is to understand the kinetics and to design a system that gives a fast condensation and an efficient separation of water droplets from the exhaust gas. Due to the high velocity of the mixing air and the flue gas, the residence time in the water recovery duct is less than one tenth of a second. It is crucial to understand the kinetics and thermodynamics of condensation due to supersaturation in order to mix with the correct amount of cooling air. Condensation typically occurs on surfaces and could be bolstered by a type of micro pin fin structures at the walls according to Schmitz et al [1]. This would however require the cooled steam to come in contact with the walls which would require thorough mixing. The final separation of the water droplets from the air can be made with for example a centrifugal separator. None of the presented ideas for the mixer have been tested, to the authors knowledge, and would require a significant amount of testing in order to be able to be implemented for practical usage. The calculations carried out in this work assumed that all of the condensed water could be separated, which is an error source since there always losses.

The mixer results in Table 4.11 mostly show that there is a high requirement of cooling air for the condensation of the steam in the flue gases. The exception to this result is when all the injected steam has been condensed in the condenser (100 % case). This is however expected as the 100 % case contains less steam to extract in the mixer as only part of the water created by combustion is to be extracted. On the other hand, the 100 % case might require less mixer cooling air but it will require more cooling air for the plate heat exchanger.

Considering Table 4.11, the 75 % and 100 % case are the most feasible as it is possible to recover the amount of water needed for injection. In the 50 % case it is not possible to reach a RH of 1 or above, but one comes very close when using cold air with a Mach number of 0.85. This means that the added air together with the reached temperature impairs the extraction process. When RH > 1, water will spontaneously condense, but when RH < 1, the condensation rate will not be higher than the evaporation rate as the air is not in a saturated state.

If the results are to be followed strictly, this would mean that it is not possible to perform the complete required condensation for the 50 % case, as the water recovered does not add up to the water injected. However, it should be emphasized that the method used for performing calculations within the mixer section is not optimal, as it does not account for the real process. The temperature of the hot flue gases will probably not remain constant but instead, it will increase slightly before mixing with the cold air due to spontaneous condensation occurring. When mixing is performed and further condensation occurs, the resulting flow will probably have a higher outlet temperature if not a large amount of excess cooling air is added.

The consequence of having a higher outlet mixture temperature, compared to a constant temperature, is that a lower amount of cooling air is required which benefits the system. We found that it was difficult to estimate any condensation rates or to determine any resulting mixture temperature with condensation occurring simultaneously as mixing, and for these reasons the temperature of the cold turbine exhaust flow was set to constant. Considering the stated points about the outlet temperature being higher, the 50 % case could possibly work. By using this case the condenser would be smaller, which is a benefit, but even if the 50 % case would be possible, it is still subject of demanding an enormous amount of cooling air later in the mixer compared to the other cases investigated at the same extraction level. Even with the discussion that the temperature prior to mixing and post mixing would increase, which will decrease the air flow required, it will still require more air compared to the other cases as they too will have a decrease in air flow requirements.

The case of 75 % is nearly viable when using a Mach number of 0.5 with a RH value slightly below 1, and with the potential to extract 43 % of the created water from the combustion process when using a Mach number of 0.85. This however requires a large flow of air. Considering the 100 % case, the mixer section would then only be responsible for separating the additional water, created by the combustion. This part is not very large compared to the injected water, but from Table 4.11 it can be seen the cooling air flow increases a lot as more additional, created, water is to be extracted. The huge amount of cooling air required to extract the created water, which constitutes a small portion compared to the injected water, is attributed to lower turbine exhaust outlet temperature, and thus a smaller temperature rise of the cooling air is achieved. The problem is not as significant in the other cases as in the 100 % case, as the cold turbine outlet temperature is higher for the other cases. Calculations indicate that the amount of cold air required to extract the created water in the 100 % case in the mixer increases fast as more extraction is pursued. The reason is the low partial pressure of the remaining water in the exhaust gas and in order to keep the relative humidity above 1, large amounts of cooling air must be supplied to the mixer.

It is a desirable benefit to extract the created water as it would decrease the amount of water vapor released to the atmosphere. It should be noted that by implementing the WET cycle, a small reduction of the created water vapor is already achieved as the cycle has a lower SFC. One solution could be to increase the temperature of the flue gases entering the cold turbine which in turn allows the cold air to be heated to a higher temperature, and thus a lower mass flow of cold air is needed. For example this could be achieved by using an additional heat exchanger that is used to preheat the hot gas prior to entering the cold turbine by using the hot HRSG exhaust flue gases. This would in turn also lower the original plate heat exchanger size as the cooler section would decrease due to the lower inlet temperature of the hot flue gas. This implication is however a result of the chosen methodology and can not be stated as a clear solution. This implication also emphasizes the importance of further investigation of the kinetics and thermodynamics of condensation in the mixer, in order to achieve more correct results.

One notion is that the choice of heat exchanger architecture might affect what sort of mixer situation that will occur. The crossflow heat exchangers are probably the easiest to implement in an airplane and the smallest, compared to counter current heat exchangers of the same case (50-/75-/100 %). They do however require large air flows which is not beneficial for the general performance of the aircraft. A WET engine designer might still want to chose a counter current heat exchanger due to the lower air requirement and accept the penalty of an increased weight. If there would be limit on the maximum secondary fan intake, using a crossflow heat exchanger might reduce the possibility of condensing the required amount of water in the recovery system, thus making it impossible to extract enough water for the cycle.

One important aspect that has not been properly solved due to the lack of understanding of the condensation process is the formation of ice. In several cases, the water recovery section operates at static temperatures below the freezing point, which means that ice formation could occur at the inlets of a water collector. Note that the word "could" is used, and this is due to the fact that the residence time within the mixer is so brief that it is not properly understood if steam will have time to freeze. If freezing occurs, it might affect the ability to recover water properly. Ice formation and layer build up on the mixer wall is also a possible problem which could affect the entire mixer section and affect the proper function of the water recovery. This is something that needs to be accounted for in future studies.

Water vapor at ambient conditions at the investigated altitude was neglected as it was considered to be relatively small compared to the vapor in the flue gases. In further studies, this would be of interest as it might affect the extraction in the mixer section.

5.5 Thrust generation and cycle performance

As can be seen in section 4.2.4 the thrust increases from the plate heat exchanger cold side nozzle when a higher extraction case is applied. This is expected as a higher extraction case requires more air. Also, it can be seen that the total thrust generated, and SFC achieved, is better when the plate heat exchanger is designed for a low cold side pressure drop. However, this comes at the expense of an increased heat exchanger weight. If the heat exchanger is designed for a higher heat transfer, meaning lower weight, and a higher pressure drop is allowed, the SFC increases beyond the reference GEnx SFC for all feasible cases and is thus not an option. However, if the condenser is designed for a lower pressure drop, it can be seen that the SFC is improved in relation to the reference GEnx case for all cases. An interesting result that is observed is that the SFC is greatly reduced compared to the GEnx case for the 50 % case. The reason for this is unknown, but it is partly explained by the greater mass flow through the mixer. However, it is important to highlight that the 50 % case results in a relative humidity below 1, and thus the case can not be considered functional as enough water to sustain the cycle can not be extracted.

For the 75 % case, the estimated SFC reduction in this work, in relation to our reference cycle, was found to be 12 % - 15 % while the article states that 19 % - 28 % is possible, in relation to a 2015 reference engine [2]. However, the article does not state how much water is condensed in the plate heat exchanger and how much that is condensed in the mixer. The SFC reduction reported by the article can be achieved if an extraction between 50 % and 75 % would be performed, which is possible as the 50 % case was found to be close to the lower limit and it had a SFC reduction of almost 20 % compared to our reference cycle. If a higher amount of created water is to be extracted, a higher degree of condensation should be performed in the condenser since mixing reduces the partial pressure of water left in the exhaust flow. The results indicate that a higher degree of condensation in the condenser leads to a lower SFC reduction, but it is still below the reference GEnx SFC. This means that there is potential to reduce up to 93 % of the created water from combustion and still gain a SFC reduction. The article from MTU [1] also states that a fuel reduction of 30 % can be achieved, which is close to the fuel reduction seen in this work (22 %). This would mean a decrease of CO_2 emissions, but no quantitative studies regarding CO_2 emissions were performed in this work. It is important to include the thrust reduction for the different cases as this might affect the feasibility of the WET cycle implementation. In order to reduce up to 93 % of emitted water requires a large heat exchanger, and with the reduced thrust it might not be functional.

6
Conclusion

The primary aim of this project was to investigate the potential of the WET cycle concept from a thermodynamical perspective. The modelling involved the designing of two heat exchangers and modifying the GEnx turbofan cycle to model the WET cycle. Potential major problems with the modelling were to be identified and explained.

Results from the different investigated cases indicate that from a thermodynamical perspective it may be possible to implement the WET cycle. The calculations are however based on many assumptions and most likely contain a large number of error sources. A major problem is the uncertainty of the magnitude of the error sources.

The designed heat exchangers were a heat recovery steam generator and a condenser in the form of a plate heat exchanger. The HRSG design was straight forward and results show that it could be designed with a weight of approximately 630 kg. The plate heat exchanger was designed for several different configurations and degrees of condensation but all different designs resulted in a minimal weight of approximately 3700 kg.

Performance results show that the plate heat exchanger in the water recovery step needs to extract slightly more than 50% of the injected water to be self sufficient, which also provides a greatly reduced SFC compared to reference GEnx data. The results show that it is desired to condense the minimum possible amount of water in the condenser for a better reduction of SFC, while the rest is to be condensed in the mixer. The drawback of condensing less in the plate heat exchanger is that no additional created water from the combustion can be extracted. By not extracting created water, the emission reduction will not be as high but it still exists as the WET cycle has a lower fuel consumption compared to the reference engine. However, if a larger amount of water is extracted in the condenser, there is good potential to extract the created water from combustion. This would then require a larger and heavier condenser which is not desired. Results show that all of the injected water and up to 93% of the created water can be extracted. The benefit seen by extracting only the amount required to uphold the cycle, i.e., the injected water, is that a higher SFC reduction is attained. However, the SFC reduction when extracting more water puts the cycle SFC still below the reference GEnx SFC. It is important to highlight that the designed WET cycle was not optimized and any solid quantitative conclusions can not be drawn.

The main problem of the implementation of the WET cycle concept is the lack of understanding of the process in the mixer. No accurate studies of the kinetics and thermodynamics of the process were found, which lead to further assumptions. Results imply that a higher degree of condensation in the mixer is more effective, but this could be a consequence of not having accurate methods of predicting potential problems in the mixer.

The final conclusion of the project is that even though theoretical results indicate that it is possible to implement the WET concept, implementing it practically in reality will require further studies of the processes. The performance of the mixer must be thoroughly investigated in order to successfully implement the WET concept in the future.

Bibliography

[1] Schmitz, O., Klingels, H., and Kufner, P. (January 13, 2021). "Aero Engine Concepts Beyond 2030: Part 1—The Steam Injecting and Recovering Aero Engine." ASME. J. Eng. Gas Turbines Power. February 2021; 143(2): 021001. DOI: https://doi.org/10.1115/1.4048985

[2] Pouzolz, R., Schmitz, O., Klingels, H. (2021) Evaluation of the Climate Impact Reduction Potential of the Water-Enhanced Turbofan (WET) Concept. Aerospace 2021, 8, 59. https://doi.org/10.3390/aerospace8030059

[3] Advisory Council for Aviation Research and Innovation in Europe (ACARE) (2011)

[4] Overton J. The Growth in Greenhouse Gas Emissions from Commercial Aviation, EESI, url: https://www.eesi.org/papers/view/fact-sheet-the-growth-in-greenhouse-gas-emissions-from-commercial-aviation [accessed: 2021-04-23]

[5] Air Transport Action Group (ATAG) (2011), "The right flightpath to reduce aviation emissions," Durban, South Africa.

[6] Minnis P. et. al., "Contrails, Cirrus Trends, and Climate", American Meteorological Society (2003).

[7] Kärcher, B. Formation and radiative forcing of contrail cirrus. Nat Commun 9, 1824 (2018). https://doi.org/10.1038/s41467-018-04068-0

[8] D.S. Lee, D.W. Fahey, A. Skowron, M.R. Allen, U. Burkhardt, Q. Chen, S.J. Doherty, S. Freeman, P.M. Forster, J. Fuglestvedt, A. Gettelman, R.R. De León, L.L. Lim, M.T. Lund, R.J. Millar, B. Owen, J.E. Penner, G. Pitari, M.J. Prather, R. Sausen, L.J. Wilcox (2021), The contribution of global aviation to anthropogenic climate forcing for 2000 to 2018, Atmospheric Environment, Volume 244, 117834, ISSN 1352-2310, https://doi.org/10.1016/j.atmosenv.2020.117834.

[9] MTU Aero Engines AG, Klingels H. (2019) Request for patent for the proposed concept. Deutches Patent- und Markenamt. Patent number: DE 10 2019 203 595 A1.

[10] H. I. H. Saravanamutto, G. F. C. Rogers, H. Cohen et al. (2008) Gas Turbine Theory (6th ed.) Pearson Prentice Hall.

[11] Thunman H. (2020), MEN031 Combustion Engineering, Chemical thermodynamics, chapter 3.1. Department of Energy and Environment, Chalmers University of Technology.

[12] S. L. Dixon & C. A. Hall (2014) Fluid Mechanics and Thermodynamics of Turbomachinery (7th ed.). Elsevier.

[13] Grönstedt T. (2000), Development of methods for analysis and optimization of complex jet engine systems, Doctoral thesis, Chalmers University of Technology. ISBN: 91-7197-910-7.

[14] M. Jonsson & J.Yan (2005). Humidified Gas Turbines - a review of proposed and implemented cycles. Pages 1013 - 1078 In Sciencedirect. DOI: https://doi.org/10.1016/j.energy.2004.08.005.

[15] Henneberry H. M. & Snyder C. A. (July 1993). Analysis of Gas Turbine Engine Using Water and Oxygen Injection to Achieve High Mach Numbers and High Thrust. NASA. Accessed via ResearchGate (Accessed 2021 - 04 - 20).

[16] Thomas W. Wild, Ph.D. Aircraft Powerplants, Ninth Edition. WATER INJECTION, Chapter (McGraw-Hill Education: New York, Chicago, San Francisco, Athens, London, Madrid, Mexico City, Milan, New Delhi, Singapore, Sydney, Toronto, 2018). https://www-accessengineeringlibrary-com.proxy.lib.chalmers.se/content/book/9781259835704/toc-chapter/chapter6/section/section79

[17] Thomas W. Wild, Ph.D. Aircraft Powerplants, Ninth Edition. GAS-TURBINE ENGINE PERFORMANCE, Chapter (McGraw-Hill Education: New York, Chicago, San Francisco, Athens, London, Madrid, Mexico City, Milan, New Delhi, Singapore, Sydney, Toronto, 2018). https://www.accessengineeringlibrary.com/content/book/9781259835704/toc-chapter/chapter12/section/section12

[18] Buck, A. (1981). New Equations for Computing Vapor Pressure and Enhancement Factor. Journal of Applied Meterology and Climatology: Vol. 20. DOI: https://doi.org/10.1175/1520-0450(1981)020%3C1527:NEFCVP%3E2.0.CO;2.

[19] Sadraey, Mohammad H.. (2017). Aircraft Performance - An Engineering Approach. CRC Press. Retrieved from https://app.knovel.com/hotlink/toc/id:kpAPAEA006/aircraft-performance/aircraft-performance

[20] K.W. McGill (2017). Heat Recovery Steam Generator Technology Chapter 10 - Mechanical Design. Woodhead Publishing. ISBN: 978-0-08-101940-5.

[21] J.H Lienhard IV, J.H Lienhard V. (2017) A Heat Transfer Textbook (4th ed.) Phlogiston Press.

[22] Gnielinski, Volker (2010). Part G. VDI Heat Atlas (2nd ed.). Springer.

[23] Sinnott, Ray, et al. Chemical Engineering Design : Chemical Engineering Volume 6, Chapter 12, Elsevier Science & Technology, 2005. ProQuest Ebook Central.

[24] Kind M. et al. (2010) H3 Flow Boiling. In: VDI e. V. (eds) VDI Heat Atlas. VDI-Buch. Springer, Berlin, Heidelberg.

[25] Kast, Werner (2010). Part L. VDI Heat Atlas (2nd ed.). Springer.

[26] Elliot J. R., Lira C. T. (2009) Introductory Chemical Engineering Thermodynamics, Prentice Hall, ISBN: 0-13-011386-7.

[27] Coulson and Richardson's Chemical Engineering : Volume 1A: Fluid Flow: Fundamentals and Applications, Chapter 3, Elsevier Science & Technology, 2017. ProQuest Ebook Central.

[28] Holger Martin, A theoretical approach to predict the performance of chevron-type plate heat exchangers, Chemical Engineering and Processing: Process

Intensification, Volume 35, Issue 4, 1996, Pages 301-310, ISSN 0255-2701, https://doi.org/10.1016/0255-2701(95)04129-X.

[29] Thulukkanam, K. (2013). Heat Exchanger Design Handbook (2nd ed.). CRC Press. https://doi.org/10.1201/b14877

[30] Towler, Gavin, and Ray Sinnott. Chemical Engineering Design : Principles, Practice and Economics of Plant and Process Design, Elsevier Science & Technology, 2012.

[31] Shah, Ramesh K. Sekulić, Dušan P.. (2003). Fundamentals of Heat Exchanger Design - 3.7.2 Log-Mean Temperature Difference Correction Factor F. John Wiley & Sons.

[32] Shah, Ramesh K. Sekulić, Dušan P.. (2003). Fundamentals of Heat Exchanger Design - 3.5.2 Number of Transfer Units, NTU. John Wiley & Sons.

[33] Magnus Holmgren (2021). X Steam, Thermodynamic properties of water and steam.

[34] Anders Lundbladh (thesis supervisor), Internal communication (2021), GKN Aerospace.

[35] Xue R. et al. Effect of steam addition on gas turbine combustor design and performance (2016). Applied Thermal Engineering, Vol 104, pp. 249-257. DOI: 10.1016/j.applthermaleng.2016.05.019

[36] Zeller M., Busweiler U. (2010) M8 Humidifying and Drying of Air. In: VDI e. V. (eds) VDI Heat Atlas. VDI-Buch. Springer, Berlin, Heidelberg.

[37] Engineering ToolBox, (2014). Gases - Dynamic Viscosity. [online] Available at: https://www.engineeringtoolbox.com/gases-absolute-dynamic-viscosity-d_1888.html [Accessed continuously during spring 2021].

[38] Sjögren, O, Xisto, C Grönstedt, T. "Estimation of Design Parameters and Performance for a State-of-the-Art Turbofan." Proceedings of the ASME Turbo Expo 2021: Turbomachinery Technical Conference and Exposition. Virtual, Online. June 7–11, 2021. GT2021-59489

[39] Alfa Laval, The theory behind heat transfer, Available at: https://www.alfalaval.com/globalassets/documents/microsites/heating-and-cooling-hub/alfa_laval_heating_and_cooling_hub_the_theory_behind_heat_transfer.pdf [Accessed May 2021].

A

Appendix

A.1 Heat Recovery Steam Generator

The calculated heat transfer coefficients can be found in table A.1

Table A.1: Heat transfer coefficients for the HRSG segments for both tube and shell side.

Part	h_{fg} $[W/(m^2K)]$	h_{H_2O} $[W/(m^2K)]$	U $[W/(m^2K)]$
Economizer	326.19	6387.79	309.72
Evaporator	326.19	21259	320.60
Superheater	326.19	1048.3	248.38

The calculated HRSG dimensions are shown in Table A.2 and the designations are explained in the accompanying Figure A.1. The orange arrows represent the flue gases exiting the low pressure turbine and the circles represents the cross section of the tubes surrounding the conical structure. Table A.3 shows fluid properties in the tube banks of the HRSG. Figure 3.1 shows area parameters and velocities through the tube banks of the conical HRSG.

Table A.2: Calculated and set dimensions for the HRSG cone structure.

Pipes x-axis [Pieces]	Pipes y-axis [Pieces]	L_1 [m]	L_2 [m]	L_3 [m]	P_t [1]
129	23	2	1.89	2.14	$1.4D_o$

[1] P_t is the pitch diameter. A triangular pitch has been chosen in this work.

Table A.3: Area specifications of conical HRSG and flue gas velocity.

$Area_1$ $[m^2]$	$Area_2$ $[m^2]$	v_1 [m/s]	v_2 [m/s]	v_{avrg} [m/s]
6.72	10.2	69.23	26.76	47.99

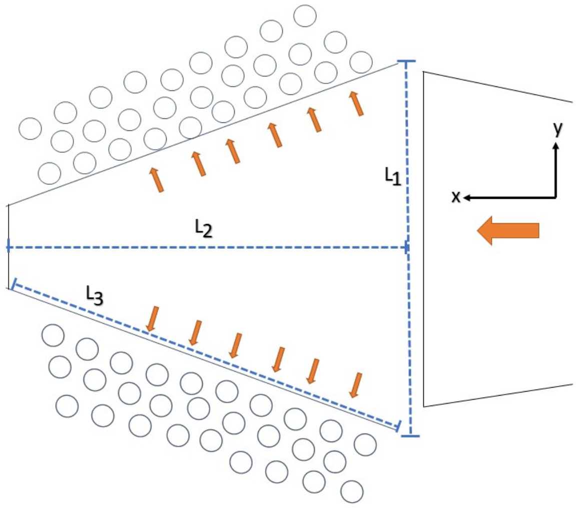

Figure A.1: Depiction of the cone-shaped HRSG as supporting Figure for designations in Table A.2.

A.2 Plate Heat Exchanger

In table A.4 the inlet and outlet temperatures obtained for the different designs is shown. Note that the table is split into a cooler and a condenser section.

Table A.4: Inlet and outlet temperatures for the different heat exchanger architectures with $\Delta T_{pinch} = 5$K.

Case - Cooler	T_{hot}^{in} [K]	T_{hot}^{out} [K]	T_{cold}^{in} [K]	T_{cold}^{out} [K]
1-pass/1-pass Crossflow	530.64	334.25	254	324.25
1-pass/2-pass Crossflow	530.64	334.25	308.95	349.53
Countercurrent 50%	530.64	334.25	329	413
Countercurrent 75%	530.64	334.25	329	384.5
Countercurrent 100%	530.64	334.25	329	370
Case - Condenser	T_{hot}^{in}	T_{hot}^{out}	T_{cold}^{in}	T_{cold}^{out}
1-pass/1-pass Crossflow	334.25	318.95	254	308.95
1-pass/2-pass Crossflow	334.25	318.95	254	308.95
Countercurrent 50%	334.25	325.95	254	329
Countercurrent 75%	334.25	318.95	254	329
Countercurrent 100%	334.25	306.05	254	329

Table A.5 presents the obtained dimensions for the different plate heat exchanger designs. See Figure A.2 for a graphical orientation of the plates.

The crossflow heat exchangers use a $\Delta T_{pinch} = 10$K while the countercurrent are tuned to $\Delta T_{pinch} = 5$K if not specified otherwise.

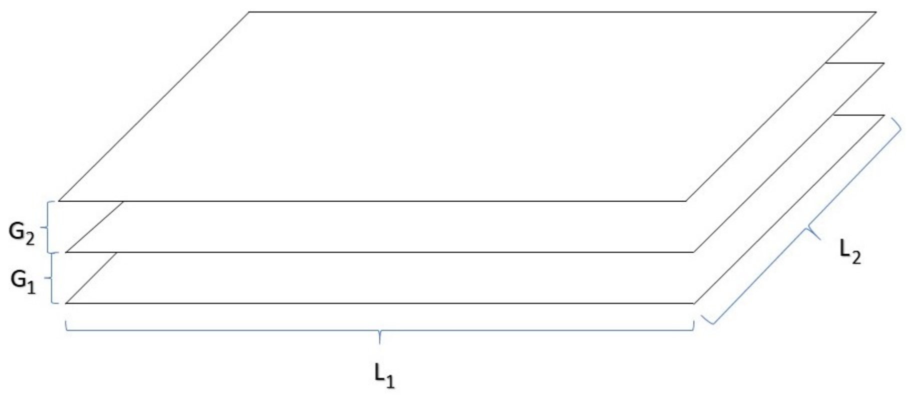

Figure A.2: Graphical representation of stacked plates and dimensional orientation.

Table A.5: Obtained plate heat exchanger dimensions and fluid travel length.

Architecture Higher U	$G_{1,hot}^{cooler}$ [m]	$G_{2,cold}^{cooler}$ [m]	$G_{1,hot}^{condenser}$ [m]	$G_{2,cold}^{condenser}$ [m]
1-Pass/1-Pass Crossflow 75%	0.0264	0.025	0.0105	0.015
1-Pass/2-Pass Crossflow 75%	0.0155	0.021	0.0106	0.0245
Countercurrent 50%	0.00655	0.005	0.0062	0.01
Countercurrent 75%, ΔT = 10K	0.009	0.02	0.005	0.012
Countercurrent 75%, ΔT = 5K	0.00815	0.016	0.0042	0.01
CounterCurrent 100%	0.0083	0.02	0.0035	0.009
Architecture Lower ΔP_c	$G_{1,hot}^{cooler}$ [m]	$G_{2,cold}^{cooler}$ [m]	$G_{1,hot}^{condenser}$ [m]	$G_{2,cold}^{condenser}$ [m]
CounterCurrent 50%,	0.0063	0.015	0.0055	0.012
CounterCurrent 75%	0.00695	0.022	0.0042	0.0105
Countercurrent 100%	0.0095	0.022	0.0028	0.012

The number of plates for each architecture is shown in table A.6.

Table A.6: Number of plates for different plate heat exchanger architecture.

Architecture Higher U	$\#_{plates,cooler}$	$\#_{plates,condenser}$
1-Pass/1-Pass Crossflow 75%	73	347
1-Pass/2-Pass Crossflow 75%	167	347
Countercurrent 50%	232	335
Countercurrent 75%, ΔT = 10K	150	421
Countercurrent 75%, ΔT = 5K	205	525
Countercurrent 100%	167	843
Architecture Lower ΔP_c	$\#_{plates,cooler}$	$\#_{plates,condenser}$
Countercurrent 50%	283	358
Countercurrent 75%	248	558
Countercurrent 100%	239	912

The area of the plates was set to 8 m^2 where L_1 = 4m and L_2 = 2m. The travel length for each fluid for the different architectures is shown in table A.7.

Table A.7: Travel length for the fluids in the different plate heat exchanger architectures.

Architecture	L_{hot}	L_{cold}
1-Pass/1-Pass Crossflow	2x L_1 = 8m	L_2 = 2m
1-Pass/2-Pass Crossflow	2x L_1 = 8m	2x L_2 = 4m
Countercurrent	2x L_2 = 4m	2x L_2 = 4m

Table A.8 shows the obtained overall heat transfer coefficients, U, for the different parts of the condenser (cooling or condensing part) and if needed, the correction factor for the given part.

Table A.8: Overall heat transfer coefficients obtained for the investigated architectures and correction factors for crossflow heat exchangers.

Architecture Higher U	$U_{cooling}$ $[W/m^2K]$	$U_{condensing}$ $[W/m^2K]$	F_{cooler}	$F_{condenser}$
1-Pass/1-Pass Crossflow 75%	106	97	0.860	0.916
1-Pass/2-Pass Crossflow 75%	104	91	0.646	0.916
Countercurrent 50%	106	95	1	1
Countercurrent 75%, ΔT = 10K	112	98	1	1
Countercurrent 75%, ΔT = 5K	104	99	1	1
Countercurrent 100%	117.5	92	1	1
Architecture Lower ΔP_c	$U_{cooling}$ $[W/m^2K]$	$U_{condensing}$ $[W/m^2K]$	F_{cooler}	$F_{condenser}$
Countercurrent 50%	87	89	1	1
Countercurrent 75%	86	93	1	1
Countercurrent 100%	82	85	1	1

Gas velocities for the plate heat exchanger and the investigated architectures can be found in Table A.9

Table A.9: Plate heat exchanger velocities for different investigated architectures.

Architecture Higher U	V_{hot}^{cooler} [m/s]	$V_{hot}^{condenser}$ [m/s]	V_{cold}^{cooler} [m/s]	$V_{cold}^{condenser}$ [m/s]
1-Pass/1-Pass Crossflow 75%	22.86	14.38	65.18	36.34
1-Pass/2-Pass Crossflow 75%	17.02	13.34	58.97	41.55
Countercurrent 50%	14.49	11,81	21.31	25.16
Countercurrent 75%, ΔT_{pinch} = 10K	16.32	11.65	53.83	27.33
Countercurrent 75%, ΔT_{pinch} = 5K	13.18	11.12	45.97	24.52
Countercurrent 100%	15.89	8.31	61.92	23.32
Architecture Lower ΔP_c	V_{hot}^{cooler} [m/s]	$V_{hot}^{condenser}$ [m/s]	V_{cold}^{cooler} [m/s]	$V_{cold}^{condenser}$ [m/s]
Countercurrent 50%	12.35	12.46	23.31	19.62
Countercurrent 75%	12.78	10.47	27.66	21.98
Countercurrent 100%	9.70	9.61	39.4	16.16

A.3 Secondary fan

In table A.10 the post fan temperatures are shown for all the different cases together with the found fan pressure ratio.

Table A.10: Post secondary fan temperatures for cold air flow.

Case	$M_{air(a)}$	$\dot{m}_{Extracted}$ [kg/s] (Injected/Created)	$\dot{m}_{air(a)}$ [kg/s]	PR-fan	$T_{total(a)}$ [K]	$T_{static(a)}$ [K]
100%	25	0 / 0.10	195.74	1.051	254.32	251.18
100%	25	0 / 0.25	226.15	1.0439	253.78	250.65
100%	25	0 / 0.49	274.99	1.0363	253.22	250.09
100%	0.5	0 / 0.10	196.43	1.0507	254.30	242.19
100%	0.5	0 / 0.25	227.88	1.0434	253.74	241.66
100%	0.5	0 / 0.5	280.51	1.035	253.11	241.05
100%	0.5	0 / 0.68	318.49	1.0312	252.81	240.77
100%	0.85	0 / 0.10	198.15	1.05	254.25	222.15
100%	0.85	0 / 0.25	232.19	1.0422	253.65	221.63
100%	0.85	0 / 0.5	289.17	1.0335	252.99	221.05
100%	0.85	0 / 0.70	334.89	1.0287	252.63	220.73
100%	0.85	0 / 0.90	380.67	1.0251	252.36	220.49
100%	0.85	0 / 0.93	387.65	1.0256	252.33	220.47
75%	0.25	1.3 / 0	263.21	1.0432	253.73	250.6
75%	0.5	1.3 / 0	268.11	1.04225	253.66	241.58
75%	0.85	1.3 / 0	279.52	1.0401	253.49	221.49
75%	0.85	1.3 / 0.10	292.55	1.0383	253.36	221.37
75%	0.85	1.3 / 0.25	312.11	1.0359	253.12	221.21
75%	0.85	1.3 / 0.30	318.63	1.0351	253.11	221.16
75%	0.85	1.3 / 0.48	342.64	1.0247	252.98	221.04
50%	0.25	2.61 / 0	299.49	1.0418	253.62	250.49
50%	0.5	2.61 / 0	309.73	1.0402	253.50	241.43
50%	0.85	2.61 / 0	328.49	1.0375	253.30	221.32

In table A.11 the post fan pressures are shown for all the different cases together with the found fan pressure ratio.

Table A.11: Post secondary fan pressures for cold air flow.

Case	$M_{air(a)}$	$\dot{m}_{extracted}$ (Injected/Created)	$\dot{m}_{air(a)}$ [kg/s]	PR-fan	$P_{total(a)}$ [Pa]	$P_{static(a)}$ [Pa]
100%	0.25	0 / 0.10	195.74	1.051	40108.105	38434.824
100%	0.25	0 / 0.25	226.15	1.0439	39837.156	38175.179
100%	0.25	0 / 0.49	274.99	1.0363	39547.126	37897.249
100%	0.5	0 / 0.10	196.43	1.0507	40096.657	33915.167
100%	0.5	0 / 0.25	227.88	1.0434	39818.075	33679.533
100%	0.5	0 / 0.5	280.51	1.035	39497.516	33408.392
100%	0.5	0 / 0.68	318.49	1.0312	39352.501	33285.733
100%	0.85	0 / 0.10	198.15	1.05	40069.943	25206.152
100%	0.85	0 / 0.25	232.19	1.0422	39772.281	25018.907
100%	0.85	0 / 0.5	289.17	1.0335	39440.273	24810.056
100%	0.85	0 / 0.70	334.89	1.0287	39257.096	24694.828
100%	0.85	0 / 0.90	380.67	1.0251	39119.713	24608.407
100%	0.85	0 / 0.93	387.65	1.0256	39138.794	24620.409
75%	0.25	1.3 / 0	263.21	1.0432	39810.443	38149.58
75%	0.5	1.3 / 0	268.11	1.04225	39774.189	33642.412
75%	0.85	1.3 / 0	279.52	1.0401	39693	24968.494
75%	0.85	1.3 / 0.10	292.55	1.0383	39623.45	24925.284
75%	0.85	1.3 / 0.25	312.11	1.0359	39531.861	24867.67
75%	0.85	1.3 / 0.30	318.63	1.0351	39501.332	24848.465
75%	0.85	1.3 / 0.48	342.64	1.0247	39104.449	24598.804
50%	0.25	2.61 / 0	299.49	1.0418	39757.016	38098.382
50%	0.5	2.61 / 0	309.73	1.0402	39695.957	33576.241
50%	0.85	2.61 / 0	328.49	1.0375	39592.92	24906.079

Note that both the pressure and temperature will vary depending on which case that is investigated. This is due to the fact that the cold turbine delivers a given work output and when the degree of condensations increases, the air flow increases. This leads to a decrease in fan pressure ratio.

A.4 Cold Turbine

Exhaust parameters for the cold turbine is shown in table A.12.

Table A.12: Cold turbine exhaust pressures for the different cases.

Case	$M_{air(a)}$	$\dot{m}_{extracted}$ (Injected/Created)	$P_{static(4)}$ [Pa]	$P_{total(4)}$ [Pa]
100%	0.25	0 / 0.10	38434.82	40142.79
100%	0.25	0 / 0.25	38175.18	39871.6
100%	0.25	0 / 0.49	37897.25	39581.32
100%	0.5	0 / 0.10	33915.17	40230.6
100%	0.5	0 / 0.25	33679.53	39951.09
100%	0.5	0 / 0.5	33408.39	39629.46
100%	0.5	0 / 0.68	33285.73	39483.96
100%	0.85	0 / 0.10	25206.15	40426.1
100%	0.85	0 / 0.25	25018.91	40125.79
100%	0.85	0 / 0.5	24810.06	39790.83
100%	0.85	0 / 0.70	24694.83	39606.03
100%	0.85	0 / 0.90	24608.41	39467.42
100%	0.85	0 / 0.93	24620.41	39486.67
75%	0.25	1.30 / 0	38149.58	39844.87
75%	0.5	1.30 / 0	33642.41	39907.05
75%	0.85	1.30 / 0	24968.49	40044.94
75%	0.85	1.30 / 0.10	24925.28	39975.64
75%	0.85	1.30 / 0.25	24867.67	39883.24
75%	0.85	1.30 / 0.30	24848.47	39852.43
75%	0.85	1.30 / 0.48	24598.8	39452.02
50%	0.25	2.61 / 0	38098.38	39791.39
50%	0.5	2.61 / 0	33576.24	39828.56
50%	0.85	2.61 / 0	24906.08	39944.84

The cold turbine outlet temperature (static) is shown in table A.13.

Table A.13: Cold turbine outlet temperatures (static) for all investigated cases.

Case	$M_{air(a)}$	$\dot{m}_{extracted}$ (Injected/Created)	$T_{static(4)}$ [K]
100%	0.25	0 / 0.10	264.60
100%	0.25	0 / 0.25	264.08
100%	0.25	0 / 0.49	263.53
100%	0.5	0 / 0.10	255.19
100%	0.5	0 / 0.25	254.68
100%	0.5	0 / 0.5	254.08
100%	0.5	0 / 0.68	253.81
100%	0.85	0 / 0.10	234.20
100%	0.85	0 / 0.25	233.70
100%	0.85	0 / 0.5	233.13
100%	0.85	0 / 0.70	232.82
100%	0.85	0 / 0.90	232.58
100%	0.85	0 / 0.93	232.46
75%	0.25	1.30 / 0	274.79
75%	0.5	1.30 / 0	265.00
75%	0.85	1.30 / 0	243.17
75%	0.85	1.30 / 0.10	243.05
75%	0.85	1.30 / 0.25	242.88
75%	0.85	1.30 / 0.30	242.83
75%	0.85	1.30 / 0.48	242.13
50%	0.25	2.61 / 0	280.71
50%	0.5	2.61 / 0	270.66
50%	0.85	2.61 / 0	248.33

Table A.14: Cold turbine total outlet temperatures depending on condenser extraction degree.

Case	$T_{total(4)}$ [K]
100%	265.20
75%	276.00
50%	282.06

A.5 Mixer

The data given in this section is explained in accordance to Figure A.3. Reefer to the Figure for clarification of some reported parameters.

No additional data is shown for the 50% case as all available data is shown in the results, Table 4.11.

Table A.15 shows different cases of water extraction in the mixer section when applying the case of 75% injected water condensation in the plate heat exchanger.

Table A.15: Entire mixer results for the case of 75% condensation in plate heat exchanger.

$M_{air(a)}$	$\dot{m}_{water(4)}$ [kg/s]	$\dot{m}_{extracted}$ (Injected/Created)	$X^{total}_{extracted}$	$\dot{m}_{air(a)}$ [kg/s]	$RH_{(5)}$
0.25	2.3025	1.30 / 0	0.839	135.769	0.592
0.5	2.3025	1.30 / 0	0.839	140.667	1.000
0.85	2.3025	1.30 / 0	0.839	152.083	2.093
0.85	2.3025	1.30 / 0.10	0.856	165.113	1.832
0.85	2.3025	1.30 / 0.25	0.880	184.669	1.480
0.85	2.3025	1.30 / 0.30	0.888	191.193	1.370
0.85	2.3025	1.30 / 0.48	0.917	215.203	1.020

Table A.16 shows different cases of water extraction in the mixer section when applying the case of 100% injected water condensation in the plate heat exchanger.

Table A.16: Entire mixer results for the case of 100% condensation in plate heat exchanger.

$M_{air(a)}$	$\dot{m}_{water(4)}$ [kg/s]	$\dot{m}_{extracted}$ (Injected/Created)	$X^{total}_{extracted}$	$\dot{m}_{air(a)}$ [kg/s]	$RH_{(5)}$
0.25	1	0 / 0.10	0.856	20.186	4.546
0.25	1	0 / 0.25	0.880	50.594	2.366
0.25	1	0 / 0.49	0.918	99.435	1.028
0.5	1	0 / 0.10	0.856	20.877	9.946
0.5	1	0 / 0.25	0.88	52.326	4.981
0.5	1	0 / 0.5	0.92	104.963	2.053
0.5	1	0 / 0.68	0.949	142.943	1.029
0.85	1	0 / 0.10	0.856	22.597	60.552
0.85	1	0 / 0.25	0.88	56.642	29.918
0.85	1	0 / 0.5	0.92	113.623	12.31
0.85	1	0 / 0.70	0.952	159.336	5.694
0.85	1	0 / 0.90	0.984	205.116	1.546
0.85	1	0 / 0.93	0.871	212.094	1.060

The entire exhaust mixture temperatures after condensation is shown in table A.17 for the different cases.

Table A.17: Mixture exhaust temperatures.

Case	$M_{air(a)}$	$\dot{m}_{extracted}$ (Injected/Created)	$T_{static(5)}$ [K]	$T_{total(5)}$ [K]
100%	0.25	0 / 0.10	265.24	266.29
100%	0.25	0 / 0.25	264.42	266.54
100%	0.25	0 / 0.49	263.62	266.42
100%	0.5	0 / 0.10	255.03	265.57
100%	0.5	0 / 0.25	254.58	266.19
100%	0.5	0 / 0.5	254.03	266.24
100%	0.5	0 / 0.68	253.78	266.16
100%	0.85	0 / 0.10	234.28	264.33
100%	0.85	0 / 0.25	233.87	265.67
100%	0.85	0 / 0.5	233.34	266.12
100%	0.85	0 / 0.70	233.03	266.14
100%	0.85	0 / 0.90	232.80	266.09
100%	0.85	0 / 0.93	232.68	265.99
75%	0.25	1.30 / 0	275.46	277.85
75%	0.5	1.30 / 0	265.00	274.96
75%	0.85	1.30 / 0	257.59	277.72
75%	0.85	1.30 / 0.10	256.95	277.66
75%	0.85	1.30 / 0.25	256.10	277.57
75%	0.85	1.30 / 0.30	255.84	277.54
75%	0.85	1.30 / 0.48	254.43	276.88
50%	0.25	2.61 / 0	281.22	283.96
50%	0.5	2.61 / 0	272.73	283.87
50%	0.85	2.61 / 0	260.63	283.86

The entire exhaust mixture pressures after condensation is shown in table A.18 for the different cases.

Table A.18: Mixture exhaust pressures (without duct pressure loss of 3 % taken into consideration).

Case	$M_{air(a)}$	$\dot{m}_{extracted}$ (Injected/Created)	$P_{static(5)}$ [Pa]	$P_{total(5)}$ [Pa]
100%	0.25	0 / 0	38659.64	39229.16
100%	0.25	0 / 0.25	38326.57	39448.77
100%	0.25	0 / 0.49	37953.10	39403.61
100%	0.5	0 / 0.10	33985.23	39474.310
100%	0.5	0 / 0.25	33727.90	39602.12
100%	0.5	0 / 0.5	33436.90	39488.49
100%	0.5	0 / 0.68	33308.84	39398.01
100%	0.85	0 / 0	25514.47	39780.62
100%	0.85	0 / 0.25	25241.09	39850.78
100%	0.85	0 / 0.5	24963.15	39690.03
100%	0.85	0 / 0.70	24821.53	39554.43
100%	0.85	0 / 0.90	24719.25	39440.28
100%	0.85	0 / 0.93	24670.87	39375.09
75%	0.25	1.30 / 0	38715.68	39860.15
75%	0.5	1.30 / 0	35974.04	40756.47
75%	0.85	1.30 / 0	32720.00	42246.03
75%	0.85	1.30 / 0.10	32322.62	42063.59
75%	0.85	1.30 / 0.25	31797.45	41822.22
75%	0.85	1.30 / 0.30	31636.54	41746.69
75%	0.85	1.30 / 0.48	30889.99	41220.43
50%	0.25	2.61 / 0	38530.15	39826.52
50%	0.5	2.61 / 0	35298.37	40466.68
50%	0.85	2.61 / 0	31081.05	41623.34

In table A.19, the mixture exhaust velocity and Mach number for all cases is shown.

Table A.19: Exhaust mixture velocity and Mach number.

Case	$M_{air(a)}$	$\dot{m}_{extracted}$ (Injected/Created)	$C_{exhaust(5)}$ [m/s]	$M_{exhaust(5)}$
100%	0.25	0 / 0.10	260.45	0.848
100%	0.25	0 / 0.25	260.45	0.850
100%	0.25	0 / 0.49	259.19	0.847
100%	0.5	0 / 0.10	261.65	0.854
100%	0.5	0 / 0.25	261.22	0.853
100%	0.5	0 / 0.5	259.60	0.849
100%	0.5	0 / 0.68	258.68	0.846
100%	0.85	0 / 0.10	262.88	0.861
100%	0.85	0 / 0.25	262.45	0.85878
100%	0.85	0 / 0.5	260.77	0.853
100%	0.85	0 / 0.70	259.61	0.849
100%	0.85	0 / 0.90	258.66	0.846
100%	0.85	0 / 0.93	258.17	0.844
75%	0.25	1.30 / 0	268.00	0.858
75%	0.5	1.30 / 0	272.21	0.878
75%	0.85	1.30 / 0	282.33	0.911
75%	0.85	1.30 / 0.10	281.10	0.907
75%	0.85	1.30 / 0.25	279.47	0.901
75%	0.85	1.30 / 0.30	278.96	0.899
75%	0.85	1.30 / 0.48	275.34	0.888
50%	0.25	2.61 / 0	270.37	0.856
50%	0.5	2.61 / 0	274.42	0.871
50%	0.85	2.61 / 0	281.44	0.897

In Table A.20 the calculated area and diameter of the circular pipe duct that the Mixer consists out of is shown.

Table A.20: Calculated area and diameter for a circular pipe Mixer.

Case	$M_{air(a)}$	$\dot{m}_{extracted}$ (Injected/Created)	$A_{total(5)}$ $[m^2]$	$D_{duct(5)}$ [m]
100%	0.25	0 / 0.10	1.78	0.76
100%	0.25	0 / 0.25	2.20	0.83
100%	0.25	0 / 0.49	3.23	1.01
100%	0.5	0 / 0.10	0.63	0.45
100%	0.5	0 / 0.25	1.05	0.58
100%	0.5	0 / 0.5	1.77	0.75
100%	0.5	0 / 0.68	2.29	0.85
100%	0.85	0 / 0.10	0.48	0.39
100%	0.85	0 / 0.25	0.83	0.51
100%	0.85	0 / 0.5	1.42	0.67
100%	0.85	0 / 0.70	1.90	0.78
100%	0.85	0 / 0.90	2.38	0.87
100%	0.85	0 / 0.93	2.46	0.88
75%	0.25	1.30 / 0	1.19	0.61
75%	0.5	1.30 / 0	2.32	0.86
75%	0.85	1.30 / 0	1.87	0.77
75%	0.85	1.30 / 0.10	2.01	0.80
75%	0.85	1.30 / 0.25	2.22	0.84
75%	0.85	1.30 / 0.30	2.29	0.85
75%	0.85	1.30 / 0.48	2.56	0.90
50%	0.25	2.61 / 0	6.51	1.44
50%	0.5	2.61 / 0	3.58	1.07
50%	0.85	2.61 / 0	2.90	0.96

The supplementary Figure for the reported data in this section is provided below.

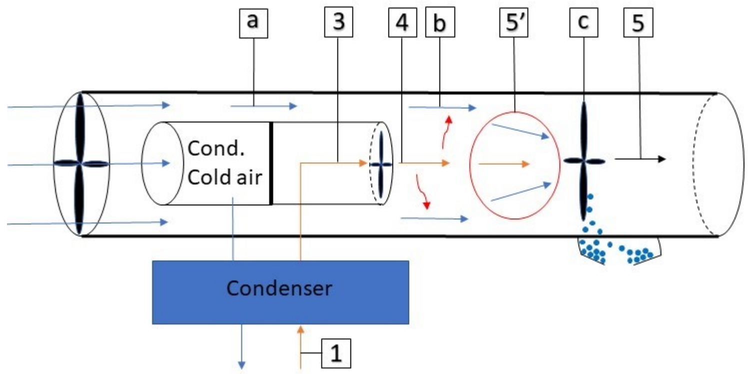

Figure A.3: The investigated mixer system

A.6 Thrust generation

The thrust generated from the mixer is shown in table A.21.

Table A.21: Thrust generated by the mixer exhaust.

Case	$M_{air(a)}$	$\dot{m}_{extracted}$ (Injected/Created)	Thrust [N]
100%	0.25	0 / 0.10	11124.3
100%	0.25	0 / 0.25	19082.9
100%	0.25	0 / 0.49	31712.5
100%	0.5	0 / 0.10	11356.4
100%	0.5	0 / 0.25	19592.0
100%	0.5	0 / 0.5	33200.4
100%	0.5	0 / 0.68	42953.6
100%	0.85	0 / 0.10	11862.0
100%	0.85	0 / 0.25	20816.8
100%	0.85	0 / 0.5	35608.3
100%	0.85	0 / 0.70	47368.4
100%	0.85	0 / 0.90	59089.4
100%	0.85	0 / 0.93	60785.3
75%	0.25	1.30 / 0	42738.9
75%	0.5	1.30 / 0	44743.4
75%	0.85	1.30 / 0	49629.6
75%	0.85	1.30 / 0.10	53000.9
75%	0.85	1.30 / 0.25	58045.4
75%	0.85	1.30 / 0.30	59721.6
75%	0.85	1.30 / 0.48	65424.4
50%	0.25	2.61 / 0	65082.7
50%	0.5	2.61 / 0	68866.3
50%	0.85	2.61 / 0	75909.7

The total net thrust generated and SFC is shown in the following two tables. Table A.22 shows total net thrust and SFC for the system containing plate heat exchanger optimized for overall heat transfer.

Table A.22: Net engine thrust and SFC for PHX optimized for overall heat transfer.

Case	$M_{air(a)}$	$\dot{m}_{extracted}$ (Injected/Created)	Thrust [N]	SFC [mg/(N s)]
100%	0.25	0 / 0.10	32862.7	23.705
100%	0.25	0 / 0.25	33157.7	23.494
100%	0.25	0 / 0.49	33478.0	23.270
100%	0.5	0 / 0.10	32920.8	23.663
100%	0.5	0 / 0.25	33230.4	23.442
100%	0.5	0 / 0.5	33572.8	23.203
100%	0.5	0 / 0.68	33754.0	23.079
100%	0.85	0 / 0.10	32992.9	23.611
100%	0.85	0 / 0.25	33367.3	23.346
100%	0.85	0 / 0.5	33798.1	23.049
100%	0.85	0 / 0.70	34037.3	22.887
100%	0.85	0 / 0.90	34220.3	22.764
100%	0.85	0 / 0.93	34157.8	22.806
75%	0.25	1.30 / 0	44599.0	17.467
75%	0.5	1.30 / 0	45368.8	17.170
75%	0.85	1.30 / 0	47378.2	16.442
75%	0.85	1.30 / 0.10	47465.4	16.412
75%	0.85	1.30 / 0.25	47581.4	16.372
75%	0.85	1.30 / 0.30	47613.1	16.361
75%	0.85	1.30 / 0.48	47265.0	16.482
50%	0.25	2.61 / 0	47136.1	16.527
50%	0.5	2.61 / 0	48338.4	16.116
50%	0.85	2.61 / 0	50653.8	15.379

Table A.23 shows total net thrust and SFC for the system containing plate heat exchanger optimized for lower cold side pressure drop.

Table A.23: Net engine thrust and SFC for PHX optimized for cold side pressure drop.

Case	$M_{air(a)}$	$\dot{m}_{extracted}$ (Injected/Created)	Thrust [N]	SFC [mg/(N s)]
100%	0.25	0 / 0.10	52015.0	14.976
100%	0.25	0 / 0.25	52310.1	14.892
100%	0.25	0 / 0.49	52630.4	14.801
100%	0.5	0 / 0.10	52073.2	14.960
100%	0.5	0 / 0.25	52382.8	14.871
100%	0.5	0 / 0.5	52725.2	14.775
100%	0.5	0 / 0.68	52906.4	14.724
100%	0.85	0 / 0.10	52145.3	14.939
100%	0.85	0 / 0.25	52519.7	14.833
100%	0.85	0 / 0.5	52950.5	14.712
100%	0.85	0 / 0.70	53189.6	14.646
100%	0.85	0 / 0.90	53372.7	14.595
100%	0.85	0 / 0.93	53310.1	14.613
75%	0.25	1.30 / 0	54729.1	14.234
75%	0.5	1.30 / 0	55499.0	14.036
75%	0.85	1.30 / 0	57508.3	13.546
75%	0.85	1.30 / 0.10	57595.6	13.525
75%	0.85	1.30 / 0.25	57711.6	13.498
75%	0.85	1.30 / 0.30	57743.2	13.491
75%	0.85	1.30 / 0.48	57395.1	13.573
50%	0.25	2.61 / 0	56870.4	13.698
50%	0.5	2.61 / 0	58072.7	13.414
50%	0.85	2.61 / 0	60388.1	12.900

DEPARTMENT OF SOME SUBJECT OR TECHNOLOGY
CHALMERS UNIVERSITY OF TECHNOLOGY
Gothenburg, Sweden
www.chalmers.se

CHALMERS
UNIVERSITY OF TECHNOLOGY